Geol. Mag. **155** (*3*), *2018, pp. 707–728.* © *Cambridge University Press 2016*
doi:10.1017/S0016756816001096

LA-ICP-MS U–Pb zircon, columbite-tantalite and ^{40}Ar–^{39}Ar muscovite age constraints for the rare-element pegmatite dykes in the Altai orogenic belt, NW China

QIFENG ZHOU*†, KEZHANG QIN*†, DONGMEI TANG*, CHUNLONG WANG*‡§ & PATRICK ASAMOAH SAKYI¶

*Key Laboratory of Mineral Resources, Institute of Geology and Geophysics, Chinese Academy of Sciences, Beijing 100029, China
‡Xinjiang Research Center for Mineral Resource, Xinjiang Institute of Ecology and Geography, Chinese Academy of Sciences, Urumqi 830011, China
§University of Chinese Academy of Sciences, Beijing 100049, China
¶Department of Earth Science, University of Ghana, PO Box LG 58, Legon-Accra, Ghana

(*Received* 23 January 2016; *accepted* 1 November 2016; *first published online* 12 December 2016)

Abstract – The Chinese Altai is renowned for its rich rare-element resources. Nine representative rare-element (REL) pegmatites were dated using LA-ICP-MS and ^{40}Ar–^{39}Ar methods. The columbite grains yield a weighted mean $^{206}Pb/^{238}U$ age of 239.6 ± 3.8 Ma for the Dakalasu (Be-Nb-Ta) pegmatite and concordia U–Pb ages of 258.1 ± 3.1 Ma and 262.3 ± 2.5 Ma for the Xiaokalasu (Li-Nb-Ta) pegmatite. The zircons display a weighted mean $^{206}Pb/^{238}U$ age of 198.5 ± 2.5 Ma for the Husite (Be) pegmatite and concordia U–Pb ages of 194.3 ± 1.6 Ma and 248.2 ± 2.2 Ma for the Qunkuer (Be) and Taerlang (barren) pegmatites. The muscovite ^{40}Ar–^{39}Ar dating gives plateau ages of 286.4 ± 1.6 Ma, 297.0 ± 2.6 Ma, 265.2 ± 1.5 Ma, 178.8 ± 1.0 Ma, 162.2 ± 0.9 Ma, 237.7 ± 1.3 Ma, 237.4 ± 1.2 Ma and 231.9 ± 1.2 Ma for the Talate (Li-Be-Nb-Ta), Baicheng (Nb-Ta), Kangmunagong (barren), Husite (Be), Qunkuer (Be-Nb-Ta), Xiaokalasu (Li-Nb-Ta), Weizigou (Be) and Taerlang (barren) pegmatites, respectively. These new ages coupled with previous geochronological work suggest that the REL pegmatites in the Chinese Altai formed during early Permain – Late Jurassic time. The REL pegmatites located in the Central Altaishan terrane are younger than those in the Qiongkuer–Abagong terrane, showing a correlation with the coeval and adjacent granites. The formation of the REL pegmatites and these granites indicates frequent and strong magmatic activity in the post-orogenic and anorogenic setting. The spatial and temporal distribution of pegmatites and granites reveals a magmatism path from the SE (of age early–middle Permian), to the NW (middle Permian – Middle Triassic) and finally to the central part (Middle Triassic – Jurassic) of the Chinese Altai.

Keywords: Columbite-tantalite U–Pb age, zircon U–Pb age, muscovite ^{40}Ar–^{39}Ar age, rare-element pegmatite, Altai.

1. Introduction

The Chinese Altai is a key part of the Central Asian Orogenic Belt, the largest Phanerozoic accretionary orogenic belt in the world (Sengör *et al.* 1993; Xiao *et al.* 2004). It is famous for hosting around 100 000 pegmatite dykes and dozens of pegmatitic rare-metal mineral deposits (Zou & Li, 2006). These pegmatites are divided into three types: muscovite (476–426 Ma, Wang *et al.* 2001); muscovite-rare-element (muscovite-REL) (369 Ma, Wang *et al.* 2003, 2004); and rare-element (REL) pegmatites (275–154 Ma, Chen *et al.* 2000; Wang *et al.* 2000, 2003, 2004, 2015; Zhu, Zeng & Gu, 2006; Wang *et al.* 2007*c*; Ren *et al.* 2011; Lv *et al.* 2012; Liu *et al.* 2015; Zhou *et al.* 2015*a*). The REL pegmatites, considered as the more evolved pegmatites, are distributed in nine pegmatite fields (Zou & Li, 2006) and could be summarized by heterogeneous Li-Be-Nb-Ta-Cs-Rb-Hf mineralization. However, the range of formation ages is not well constrained and it is unclear if an evolutionary trend is observed in the geochronology data relating to rare-element pegmatites of differing mineralization types. The available geochronology could help explain the regional tectonic setting of the Chinese Altai and may also help in the exploration of REL pegmatites in the Chinese Altai.

Here, we present new data on the geochronology of the representative REL pegmatite dykes of the Chinese Altai using laser ablation inductively coupled plasma mass spectrometry (LA-ICP-MS) columbite-tantalite U–Pb, LA-ICP-MS zircon U–Pb and muscovite ^{40}Ar–^{39}Ar dating methods. On the basis of these systematic age results and previous work, we attempt to determine the formation ages of the rare-element pegmatite dykes, reveal the time frame and evolution sequence of the rare-metal mineralization of pegmatites and then shed light on the magmatic history of the Chinese Altai during post-collisional extension.

†Authors for correspondence: zhouqifeng85@163.com, kzq@mail.iggcas.ac.cn

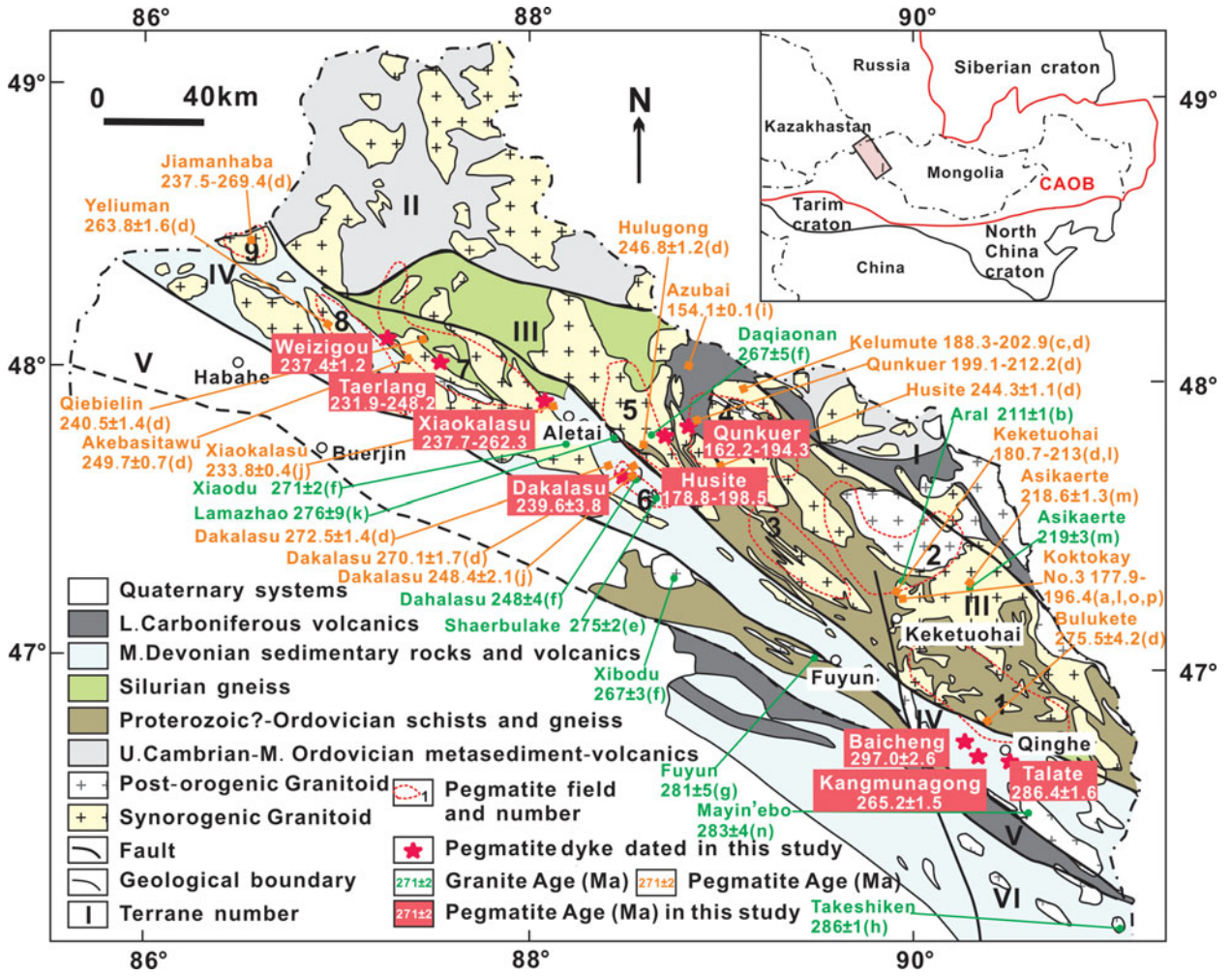

Figure 1. (Colour online) Geological sketch map of the Chinese Altai terranes, showing the locations, geological setting and formation ages of the rare-element (REL) pegmatites and related granites (modified from Luan *et al*. 1995; Windley *et al*. 2002; Wang *et al*. 2006*b*, 2007*c*; Zou & Li, 2006; Cai *et al*. 2011*a*). I, Altaishan terrane; II, NW Altaishan terrane; III, Central Altaishan terrane; IV, Qiongkuer–Abagong terrane; V, Erqis terrane; VI, Perkin–Ertai terrane. 1, Qinghe pegmatite field; 2, Keketuohai pegmatite field; 3, Kuwei–Jiebiete pegmatite field; 4, Kelumute–Jideke pegmatite field; 5, Kalaeerqisi pegmatite field; 6, Dakalasu–Kekexier pegmatite field; 7, Xiaokalasu–Qiebielin pegmatite field; 8, Hailiutan–Yeliuman pegmatite field; 9, Jiamanhaba pegmatite field. The references of ages of pegmatites and granites are a, Chen *et al*. (2000); b, Liu *et al*. (2014); c, Lv *et al*. (2012); d, Ren *et al*. (2011); e, Sun *et al*. (2009*a*) ; f, Tong (2006); g, Tong *et al*. (2006*a*) ; h, Tong *et al*. (2006*b*) ; i, Wang *et al*. (2000); j, Wang *et al*. (2003); k, Wang *et al*. (2006*b*) ; l, Wang *et al*. (2007); m, Wang *et al*. (2015); n, Zhou *et al*. (2007); o, Zhou *et al*. (2015*a*); p, Zou *et al*. (1986).

2. Geological setting

The Altai orogenic belt, comprising Mongolian, Chinese and Russian Altai, forms part of the larger Central Asian Orogenic belt (Xiao *et al*. 1992). It is situated between the Sayan and Gorny Altai of southern Siberia to the north and the Junggar block to the south (Xiao *et al*. 1992; Sengör *et al*. 1993; Jahn *et al*. 2000*a*). The Chinese Altai, composed of variably deformed and metamorphosed Vendian–Palaeozoic sedimentary, volcanic and granitic rocks (Xiao *et al*. 2009), is divided into six fault-bounded integral parts that are the Altaishan terrane, the NW Altaishan terrane, the Central Altaishan terrane, the Qiongkuer–Abagong terrane, the Erqis terrane and the Perkin–Ertai terrane (Fig. 1) (Windley *et al*. 2002). Each terrane shows different stratigraphy, metamorphism, deformation patterns and age relations (He *et al*. 1990; Qu & Zhang, 1991). The Altaishan terrane (I) consists predominantly of Middle–Upper Devonian – Carboniferous metasediments and the oldest rocks are greenschist facies (Windley *et al*. 2002; Wang *et al*. 2006*b*). The NW Altaishan terrane (II) consists largely of Neoproterozoic–Ordovician sedimentary and volcanic rocks: metasandstone, -siltstone, -shale, marble and limestone, tuff, andesitic breccia, etc. (Yuan *et al*. 2007*a*). The Central Altaishan terrane (III) contains Neoproterozoic–Silurian rocks which are amphibolite- and greenschist-facies metasediments and metavolcanics, including metasandstone, -siltstone, -shale, marble, schist, gneiss, etc. The Qiongkuer–Abagong terrane (IV) contains upper Silurian – Lower Devonian arc-type volcanic and pyroclastic rocks (Xiao *et al*. 2004) and Middle Devonian turbiditic sandstone-shale sequence (Windley *et al*. 2002). The Erqis terrane (V) is covered by Quaternary in the west and contains a high-grade gneisses and schists and Late

https://doi.org/10.1017/S0016756816001096 Published online by Cambridge University Press

Carboniferous sedimentary rocks (Windley *et al*. 2002). The Perkin–Ertai terrane (VI) consists of Devonian felsic-intermediate basic lavas and tuffs with some Carboniferous volcanics (Mei *et al*. 1993; Windley *et al*. 2002). The northern and southern parts of the Chinese Altai were formed in an arc setting, while the central parts contain no island arcs (Qin, 2000; Windley *et al*. 2002; Xiao *et al*. 2004; Qin *et al*. 2005; Wang *et al*. 2006*b*). The Chinese Altai underwent a complex process of subduction and accretion during Palaeozoic time (Xiao *et al*. 1992, 2004; Sengör *et al*. 1993; He *et al*. 1994; Windley *et al*. 2007) and finally progressed into relatively stable continent development with alternating periods of extension and compression (Li & Poliyangsiji, 2001), after finishing the formation of its basic tectonic framework no later than middle Carboniferous time (He *et al*. 1994; Windley *et al*. 2002; Li *et al*. 2003; Xiao *et al*. 2004; Wang *et al*. 2005).

Magmatism played an important role in the development of the Chinese Altai (Zou, Cao & Wu, 1989; Wang *et al*. 1998) because *c.* 200 granitoid plutons occupy at least 40 % of the Chinese Altai (Zou, Cao & Wu, 1989; Cai *et al*. 2011*b*). The emplacement of these granites took place from 479 Ma to 150 Ma discontinuously with peak ages of 460 Ma, 408 Ma, 375 Ma, 265 Ma, 210 Ma and 150 Ma (Liu, 1990, 1993; Zhang *et al*. 1996; Chen & Jahn, 2002; Wang *et al*. 2005, 2006*b*, 2007*c*, 2010, 2015; Tong *et al*. 2006*a*, *b*, 2007; Yuan *et al*. 2007*b*; Zhou *et al*. 2007; Liu *et al*. 2009, 2010*b*, 2014; Sun *et al*. 2009*a*; Chai *et al*. 2010; Li *et al*. 2010; Cai *et al*. 2011*b*; Shen *et al*. 2011). The synorogenic granites, which were emplaced earlier than 300 Ma, are widely distributed and dominant granitic intrusions in the Chinese Altai, while the post-orogenic and anorogenic granites mostly occur as small linear, approximately circular and irregular granite plutons (Fig. 1). The synorogenic granites are metaluminous to peraluminous in composition (Wang *et al*. 2006*b*; Yuan *et al*. 2007*b*; Sun *et al*. 2008; Cai *et al*. 2011*b*), derived from a mixture of continental sources and mantle-derived components (Zhao *et al*. 1993; Jahn *et al*. 2000*b*; Chen & Jahn, 2002; Wang *et al*. 2006*b*, 2009*b*; Yuan *et al*. 2007*b*; Sun *et al*. 2008, 2009*b*; Cai *et al*. 2011*a*). The post-orogenic and anorogenic granitic intrusions include biotite, two-mica and muscovite granites, monzogranite, granodiorite and syenites, etc., which belong to calc-alkaline to alkaline types with different K and Na contents (Chen & Jahn, 2002; Wang *et al*. 2005, 2015; Tong, 2006; Tong *et al*. 2006*a*, *b*; Zhou *et al*. 2007; Sun *et al*. 2009*a*; Liu *et al*. 2014). The new juvenile mantle-derived materials, besides subducted juvenile ocean crust or arc rocks, probably contributed to the generation of the post-orogenic and anorogenic granites (Wang *et al*. 2005; Tong *et al*. 2006*b*). Compared with the synorogenic granites, they were derived from a deeper crustal level where juvenile crust may predominate (Chen & Jahn, 2002). Some magma chambers experienced composite assimilation and fractional crystallization processes (Liu, Liu & Masuda, 1997; Tong, 2006). Some of the post-orogenic and anorogenic granites are spatially and temporally related to the pegmatites (Fig. 1). Geochemical research demonstrates that the source of the Aral and Asikaerte granites are possibly genetically linked to the Koktokay No. 3 and Asikaerte pegmatites, respectively (Zhu, Zeng & Gu, 2006; Zou & Li, 2006; Cao *et al*. 2013; Liu *et al*. 2014; Wang *et al*. 2015). The relationship of the post-orogenic and anorogenic granites and pegmatites in the Chinese Altai needs further research.

3. Brief review of the pegmatite dykes in the Altai orogenic belt

There are more than 100 000 pegmatite dykes in the Chinese Altai. Some of these dykes have been found to have a variety of mineralization associations: muscovite, Li, Be, Nb, Ta and Cs (Wang *et al*. 1981; Zou *et al*. 1986; Zou & Li, 2006) and have been explored. These pegmatite deposits, divided into nine pegmatite fields (Fig. 1) (Zou & Li, 2006), are concentrated in the Central Altaishan and Qiongkuer–Abagong terranes and are hosted in metagabbros, granites and metasediments. From SE to NW, the nine pegmatite fields are Qinghe (1), Keketuohai (2), Kuwei–Jiebiete (3), Kelumute–Jideke (4), Kalaeerqisi (5), Dakalasu–Kekexier (6), Xiaokalasu–Qiebielin (7), Hailiutan–Yeliuman (8) and Jiamanhaba (9) (Fig. 1) (Zou & Li, 2006). Each pegmatite field holds pegmatite deposits with different mineralization types and sizes. Three types of pegmatite deposits are identified: muscovite pegmatite, muscovite-REL (rare-element) pegmatite and REL (rare-element) pegmatite (Fig. 1). The REL pegmatite deposits include mineralization types of Li (e.g. Kukalagai in Kelumute–Jideke pegmatite field), Be (e.g. Husite and Qunkuer in Kelumute–Jideke pegmatite field), Nb-Ta (e.g. Baicheng in Qinghe pegmatite field), Be-Nb-Ta (e.g. Dakalasu in Dakalasu–Kekexier pegmatite field), Li-Nb-Ta (e.g. Xiaokalasu in Xiaokalasu–Qiebielin pegmatite field) and Li-Be-Nb-Ta-(Rb-Cs) (e.g. the Koktokay No. 3 pegmatite in Keketuohai pegmatite field) (Fig. 1). The geochronological studies show that the pegmatites in the Chinese Altai formed during Ordovician–Jurassic time (e.g. Wang *et al*. 2000, 2003, 2004; Ren *et al*. 2011; Zhou *et al*. 2015*a*). The H-O isotopes indicate that the formation of the muscovite pegmatites are characterized by incorporation of meteoritic water, while the REL pegmatites are probably from granitic magma with high $\delta^{18}O$ values (Zou & Li, 2006). The muscovite pegmatites mostly originate from metamorphic differentiation, and the muscovite-REL and REL pegmatites are genetically related to magmatic crystallization and fractionation (Zou & Li, 2006).

4. Description of the rare-element pegmatites studied

The REL pegmatite dykes investigated are located in the Qinghe, Kelumute–Jideke, Dakalasu–Kekexier and Xiaokalasu–Qiebielin pegmatite fields (Fig. 1).

https://doi.org/10.1017/S0016756816001096 Published online by Cambridge University Press

4.a. Qinghe pegmatite field

The Talate Li-Be-Nb-Ta pegmatite dyke, Baicheng Nb-Ta pegmatite dyke and barren Kangmunagong pegmatite dyke are distributed around Qinghe county in Xinjiang, NW China (Fig. 1). These pegmatite dykes occur in quartz-biotite schist. The contacts between the Talate and Baicheng pegmatites and country rocks are irregular with deformation of country rocks, while the Kangmunagong pegmatite occurs along schistosity with a sharp contact.

(1) The Talate Li-Be-Nb-Ta pegmatite dyke extends over about 150 m NW–SE, with a maximum width of 10 m and a subvertical dip to the NE. Holmquisite occurs in the altered wall rock. It shows a complex internal zoning structure. The wall zone comprises fine-grained albite-quartz-muscovite-garnet-beryl (1–2 mm) with tourmaline and columbite-tantalite as accessory minerals. Following the wall zone, the outer intermediate zone comprises graphic microcline-quartz-tourmaline intergrowth with garnet, muscovite and columbite-tantalite and coarse quartz-muscovite-beryl assemblage. The inner intermediate zone is composed of coarse (up to 30 cm in length), green spodumene and grey quartz, with aggregates of medium-grained lepidolite and cleavelandite. This grades into a core zone comprising blocky K-feldspar and milky quartz.

(2) The Baicheng Nb-Ta pegmatite dyke, 50 m long and 20 m thick with an E–W trend and subvertical dip to the north, is a lens-shaped pegmatite. It is dominated by medium–coarse-grained assemblage of K-feldspar, albite, quartz and muscovite (0.5–3 cm) that grades into blocky K-feldspar with discontinuous lenses (20 cm to 1 m in length) and the replacement zone. The lenses are composed of quartz, muscovite, albite, columbite-tantalite and green tourmaline. The replacement zone comprises saccharoidal assemblages of albite, quartz and muscovite.

(3) The Kangmunagong pegmatite dyke extends over 1 km E–W, with a maximum width of 50 m with a dip of 60° to the north. It is a relatively homogeneous body. The pegmatite is not enriched in rare elements and is formed by a coarse-grained assemblage of K-feldspar, albite, quartz and muscovite (1–3 cm), with common black tourmaline as the main accessory mineral and increasing amounts of garnet in the margins.

4.b. Kelumute–Jideke pegmatite field

The REL pegmatites studied in the Kelumute–Jideke pegmatite field are Be pegmatite dykes, referred to as Husite and Qunkuer.

(1) The Husite Be pegmatite dyke is situated 38 km SE of the township of Aletai. It extends over 700 m with a width range of 20–30 m and a NW–SE trend, and sharply cross-cuts the foliation of the schist which has an E–W trend. It shows a classic symmetrically zoned internal structure. The border zone is fine-grained assemblage of albite, quartz and muscovite (1–2 mm), followed by a wall zone of coarse muscovite-quartz-beryl-garnet that grades into an intermediate zone of blocky microcline with graphic K-feldspar-quartz intergrowth and replacement aggregate of albite.

(2) The Qunkuer Be pegmatite dyke is located 48 km ESE of the city of Aletai. The ore body has been mined and exhausted. The pegmatite cross-cuts the schist with an irregular contact. The rocks of different zones in the ore heap are saccharoidal albite-quartz-muscovite, coarse garnet and cleavelandite intergrowth, K-feldspar block, coarse-grained assemblage of muscovite (1–2 cm), smoky quartz and green beryl (0.5–2 cm in cross-section) with residual blocky K-feldspar.

4.c. Dakalasu–Kekexier pegmatite field

The REL pegmatite studied in the Dakalasu–Kekexier pegmatite field is a Be-Nb-Ta pegmatite dyke from the Dakalasu Be-Nb-Ta deposit, which is located 36 km SSE of the city of Aletai. It cross-cuts the Dahalasu porphyraceous biotite granite which is dated by zircon U–Pb method, yielding a weighted mean age of 248 ± 4 Ma (Tong, 2006). It is a symmetrically zoned dyke, *c.* 10–20 m thick and 200 m long, with a NNE–SSW trend and a gentle dip. From the contact inwards, the pegmatite consists of: (1) a border zone that is a fine-grained assemblage of albite, quartz, muscovite, garnet (1–2 mm) and tourmaline (3–5 mm in length); (2) a wall zone of graphic pegmatite with columbite-tantalite; which evolves to (3) an intermediate zone of blocky microcline-book-like aggregates of muscovite-quartz with beryl columns (up to 50 cm in length) and columbite-tantalite; and (4) a discontinuous replacement aggregate of cleavelandite situated close to (5) a quartz core (mainly white-pink quartz).

4.d. Xiaokalasu–Qiebielin pegmatite field

In the Xiaokalasu–Qiebielin pegmatite field, the Xiaokalasu (Li-Nb-Ta) and Taerlang (barren) pegmatite dykes cross-cut the quartz-biotite schist with irregular contacts, and the Weizigou (Be) pegmatite occur in two-mica granite.

(1) The Xiaokalasu Li-Nb-Ta pegmatite dyke, located 10 km SW of the city of Aletai, is *c.* 150 m long and 5–20 m wide with a N–S trend and a dip of 65–70°. In the north, it is formed of a wall zone of blocky K-feldspar with fine albite-quartz-muscovite-garnet (1–2 mm), outer intermediate zone of quartz-muscovite-K-feldspar with garnet, and inner intermediate zone of coarse-grained white-green spodumene (3–10 cm in length) -albite-quartz-muscovite with blocky K-feldspar. In the middle, it is mainly fine-grained assemblage of albite, quartz and muscovite (1–2 mm) with pink spodumene. In the south, it is formed of a wall zone of fine albite-quartz-muscovite-garnet with columbite-tantalite as accessory minerals that grades into intermediate zone of coarse white-pink

https://doi.org/10.1017/S0016756816001096 Published online by Cambridge University Press

Table 1. Descriptions of the studied samples in the Chinese Altai.

Pegmatite field	Sample	Pegmatite	Zone	Mineralogy components (wt %)	Dating method
Qinghe	TLT-2	Talate (Li-Be-Nb-Ta)	OIZ	Brl(60)-Qz(15)-Ms(10)-Ab(10)-Col-Tan(2-5)	3
	BC-4	Baicheng (Nb-Ta)	Qz-Mus-Col-Tan lens	Qz(70)-Ms(10)-Mc(10)-Ab(5)-Col-Tan(2-5)	3
	KMNG-1	Kangmunagong (Barren)	Graphic pegmatite	Mc(55-60)-Qz(25-30)-Ms(5-8)-Tur(5)-Grt(2)	3
Kelumute–Jideke	QKE-2-1	Qunkuer (Be)	Ore heap	Qz(70)-Ms(15)-Ab(10)-Brl(5)	2, 3
	HST-P	Husite (Be)	IZ	Mc(40)-Qz(45)-Ms(15)	2, 3
Dakalasu–Kekexier	12DKLS-10	Dakalsu (Be-Nb-Ta)	WZ	Mc(55)-Qz(25)-Grt(5)-Ms(5)-Col-Tan(10)	1
Xiaokalasu–Qiebielin	12XKLS-9	Xiaokalasu (Li-Nb-Ta)	IZ in the middle	Spd(15)-Ab(40)-Qz(25)-Ms(10)-Col-Tan(10)	1
	12XKLS-12	Xiaokalasu (Li-Nb-Ta)	IZ in the north	Spd(15)-Mc(25)-Ab(20)-Qz(15)-Ms(10)-Grt(5)-Col-Tan(10)	1
	XKLS-2	Xiaokalasu (Li-Nb-Ta)	IZ in the south	Ab(50-55)-Qz(15-20)-Spd(25)-Ms(10)	3
	WZG-4	Weizigou (Be)	IZ	Qz(60)-Mc(20)-Ms(10)-Brl(5)-Tur(2-5)	3
	TEL-1	Taerlang (Barren)	WZ	Ab(60)-Qz(15)-Ms(25)	2, 3

Note: The numbers in brackets represent percent contents; 1, LA-ICP-MS Columbite-Tantalite U–Pb dating; 2, LA-ICP-MS Zircon U–Pb dating; 3, Muscovite ^{40}Ar–^{39}Ar dating; WZ – wall zone; IZ – intermediate zone; OIZ – outer intermediate zone; Ab – albite; Mc – microcline; Qz – quartz; Ms – muscovite; Spd – spodumene; Brl – beryl; Col-Tan – columbite-tantalite; Tur – tourmaline; Grt – garnet.

spodumene (3–8 cm in length) -quartz-albite-muscovite with blocky K-feldspar.

(2) The Weizigou Be pegmatite dyke, situated 45 km NNE of the township of Buerjin, extends *c.* 200 m discontinuously with a maximum width of 10 m and a NE–SW trend. The country rock is two-mica granite and the thickness of the altered wall rock with tourmaline is *c.* 5–20 cm. The border zone is an assemblage of muscovite, quartz and black tourmaline. The wall zone is composed of fine albite, quartz and muscovite (1–2 mm) with black tourmaline and garnet as the accessory minerals. The intermediate zone as the main part of the pegmatite dyke is dominated by blocky K-feldspar with beryl as an accessory mineral and lenses of quartz, muscovite, beryl and green tourmaline. Locally, the blocky K-feldspar is albitized.

(3) The Taerlang barren pegmatite dyke, which is located 54 km NE of the township of Buerjin and is hosted in schist, extends over 100 m discordantly with a width of 5–10 m and an E–W trend. It is composed of a border zone of microcline-quartz-muscovite-biotite-tourmaline-garnet, and a wall zone of graphic K-feldspar-quartz intergrowth with nest-like assemblages of quartz-muscovite.

5. Samples and analytical methods

5.a. Samples and preparation

Nine pegmatite dykes with different REL-mineralization types were dated: Talate (Li-Be-Nb-Ta), Baicheng (Nb-Ta), Kangmunagong (barren), Husite (Be), Qunkuer (Be), Dakalasu (Be-Nb-Ta), Xiaokalasu (Li-Nb-Ta), Taerlang (barren) and Weizigou (Be). The samples investigated here were mainly collected from wall zone and the intermediate zone, which are mostly REL-mineralized rocks (Fig. 2). These samples are described briefly (Table 1; Fig. 2). They were analysed by columbite, zircon LA-ICP-MS U–Pb dating and muscovite ^{40}Ar–^{39}Ar dating. Samples for columbite-tantalite LA-ICP-MS U–Pb dating are 12DKLS-10, 12XKLS-9 and 12XKLS-12 (Fig. 2d, g, h). The columbite-tantalite grains collected from the wall zone of the Dakalasu pegmatite are assembled with microcline, quartz and garnet (Fig. 3a), while those collected from intermediate zones of the Xiaokalasu pegmatite are assembled with fine albite (Fig. 3b) or coarse albite (Fig. 3c). The columbite-tantalite grains are mostly euhedral crystals (Fig. 3). Samples for zircon LA-ICP-MS U–Pb dating are HST-P, QKE-2-1 and TEL-1 (Fig. 2k, c, f, respectively). Samples for muscovite ^{40}Ar–^{39}Ar dating are TLT-2, BC-4, KMNG-1, HST-P, QKE-2-1, XKLS-2, WZG-4 and TEL-1 (Fig. 2a, b, j, k, c, i, e, f, respectively).

The columbite-tantalite and zircon grains were separated, hand-picked and mounted in an epoxy resin disc. The grain mounts were then polished to expose the grains which were microphotographed in the transmitted and reflected light, and imaged by back-scattered electron (BSE) and cathodoluminescence (CL) using a LEO 1450VP SEM at the State Key Laboratory of Lithospheric Evolution, Institute of Geology and Geophysics, Chinese Academy of Sciences. These images were used to choose potential target sites for U–Pb dating and to characterize the internal features of minerals, including zones of alteration, inclusions and cracks. Samples of muscovite were crushed and sieved. About 100 mg were further purified by hand-picking under a binocular microscope to

https://doi.org/10.1017/S0016756816001096 Published online by Cambridge University Press

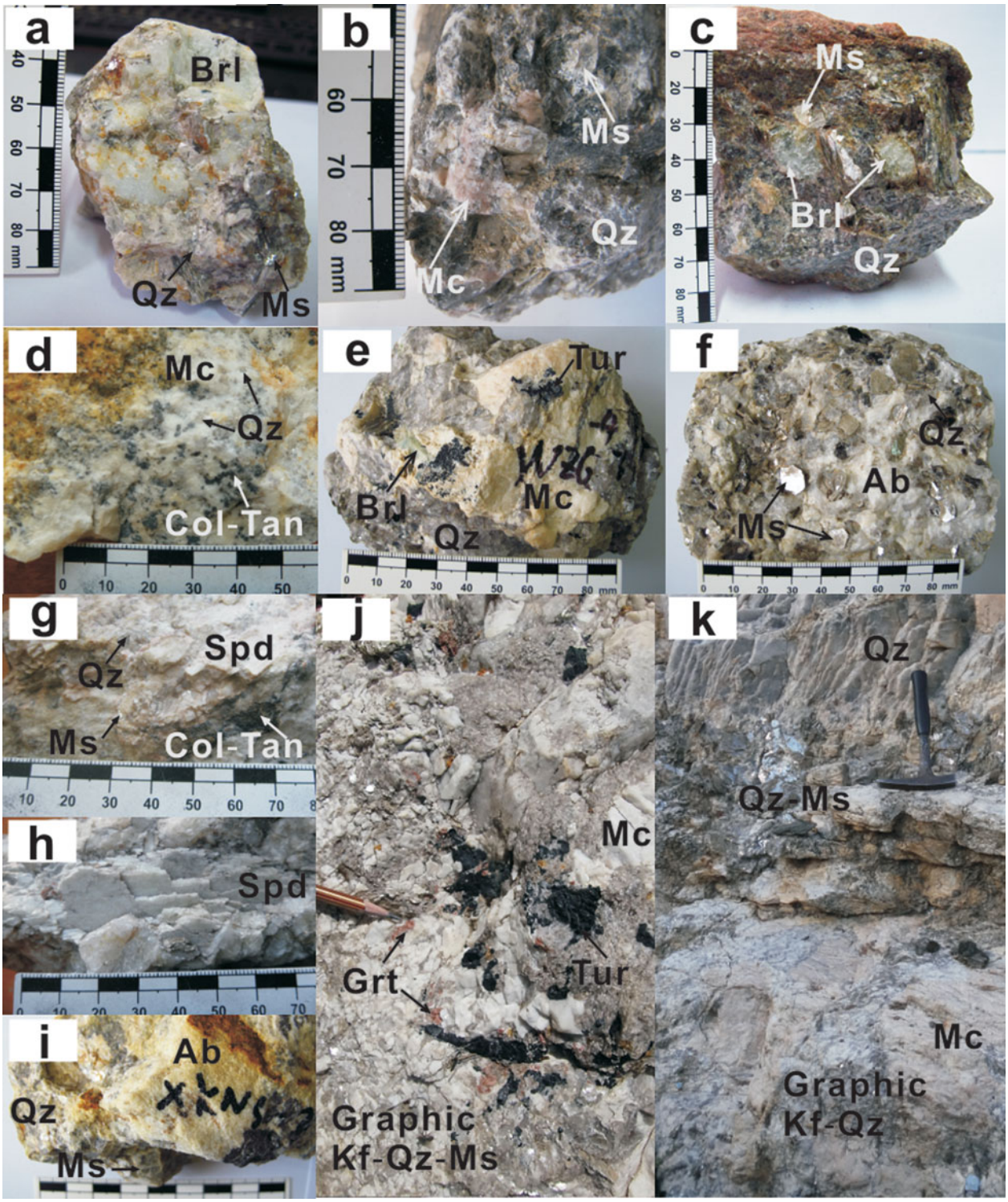

Figure 2. (Colour online) Photographs of samples: (a) TLT-2; (b) BC-4; (c) QKE-2-1; (d) 12DKLS-10; (e) WZG-4; (f) TEL-1; (g) 12XKLS-9; (h) 12XKLS-12; and (i) XKLS-2. Field images of: (j) the Kangmunagong pegmatite; and (k) internal zone of the Husite Be pegmatite. Ab – albite; Mc – microcline; Qz – quartz; Ms – muscovite; Spd – spodumene; Brl – beryl; Col-Tan – columbite-tantalite; Tur – tourmaline; Grt – garnet.

remove all visible impurities for muscovite ^{40}Ar–^{39}Ar dating.

5.b. EMPA

Major-element compositions of the columbite-tantalites in polished grain mounts were determined using a Shimadzu Corporation EPMA-1600 electron microprobe at the Laboratory of Geoanalysis and Geochronology, Tianjin Geological Survey Center, China Geological Survey. An acceleration voltage of 15 kV and a beam current of 20 nA with beam diameters of 5 μm were used for quantitative analysis. The following standards were used for the quantitative

https://doi.org/10.1017/S0016756816001096 Published online by Cambridge University Press

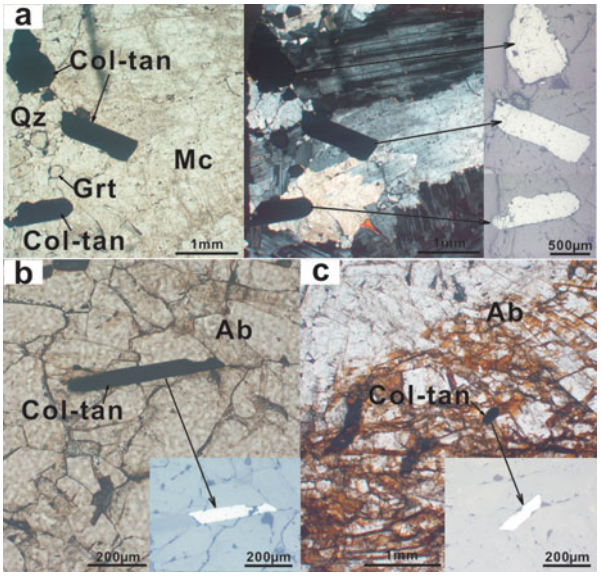

Figure 3. (Colour online) Thin-section photomicrographs of occurrences of columbite-tantalite: (a) sample 12DKLS-10, columbite-tantalite grains associate with microcline, quartz, and garnet; (b) sample 12XKLS-9, intergrowth of columbite-tantalite grains and fine-grained albite; (c) sample 12XKLS-12, columbite-tantalite associate with coarse-grained albite. Ab – albite; Mc – microcline; Qz – quartz; Col-Tan – columbite-tantalite; Grt – garnet.

analyses: scheelite (W-Kα), $LiTaO_3$ (Ta-Kα), $LiNbO_3$ (Nb-Kα), rutile (Ti-Kα), ZrO_2 (Zr-Kα), cassiterite (Sn-Kα), YP_5O_{14} (Y-Kα), Sb_2S_3 (Sb-Kα), garnet (Fe-Kα), bustamite (Mn-Kα), diopside (Ca- Kα) and PbS (Pb-Kα). Peaks and backgrounds were measured with counting times of 20 s or 40 s per element. The ZAF routine was used for data reduction (Armstrong, 1989).

5.c. LA-ICP-MS U–Pb analyses

5.c.1. LA-ICP-MS columbite-tantalite U–Pb dating

U–Pb isotopic analyses were carried out on an Agilent 7500a Q-ICPMS with a 193 nm laser ablation system hosted at the Institute of Geology and Geophysics, Chinese Academy of Sciences in Beijing. A detailed description of the Q-ICPMS can be found in Xie *et al.* (2008). To monitor the stability of the instrument and to ensure the reliability of the measured results the zircon standards (91500 and GJ-1), the coltan standard (Coltan 139) and the standard (NIST SRM 610) were measured once for every five sample points. Coltan 139 is a large unzoned columbite-(Fe) crystal from an unknown loacation in Madagascar (Gäbler *et al.* 2011; Che *et al.* 2015*a*, *b*; Melcher *et al.* 2015). It is used as an in-house reference sample by the Federal Institute for Geosciences and Natural Resources, Germany (Gäbler *et al.* 2011), and yielded an age of *c.* 506 Ma on the basis of TIMS and LA-ICP-MS dating (Melcher *et al.* 2015). In this study, $^{207}Pb/^{206}Pb$, $^{206}Pb/^{238}U$, $^{207}U/^{235}U$ ($^{235}U=^{238}U/137.88$) and $^{208}Pb/^{232}Th$ ratios were corrected using the Coltan 139 as the external standard. The fractionation correction and results were calculated using GLITTER 4.0 (Macquarie University). All of the measured isotope ratios of Coltan 139 during the process of sample analysis were regressed and corrected using reference values. The relative standard deviations of reference values for Coltan 139 were set at 2 % (Che *et al.* 2015*a*). The Concordia and weighted mean U–Pb ages were processed using ISOPLOT/Ex Version 3.0 (Ludwig, 2003). The contents of U, Th and Pb were also calculated by GLITTER 4.0, with ^{93}Nb as the internal standard and NIST 610 as an external reference material.

5.c.2. LA-ICP-MS zircon U–Pb dating

U–Pb dating analyses of zircon were conducted by LA-ICP-MS at the State Key Laboratory of Geological Processes and Mineral Resources, China University of Geosciences, Wuhan. Detailed operating conditions for the laser ablation system and the ICP-MS instrument and data reduction are the same as those described by Liu *et al.* (2008, 2010*c*) and Hu *et al.* (2008). Each analysis incorporated a background acquisition of approximately 20–30 s (gas blank) followed by 50 s data acquisition from the sample. The Agilent Chemstation was utilized for the acquisition of each individual analysis. Off-line selection and integration of background and analyte signals, as well as time-drift correction and quantitative calibration for trace-element analyses and U–Pb dating, were performed by ICPMS DataCal (Liu *et al.* 2008, 2010*c*).

Zircon 91500 was used as external standard for U–Pb dating, and was analysed twice every five analyses. Time-dependent drifts of U-Th-Pb isotopic ratios were corrected using a linear interpolation (with time) for every five analyses according to the variations of 91500 (Liu *et al.* 2010*c*). Preferred U-Th-Pb isotopic ratios used for 91500 are from Wiedenbeck *et al.* (1995). The uncertainty of the preferred values for the external standard 91500 was propagated to the ultimate results of the samples. Concordia diagrams and weighted mean calculations were achieved using Isoplot/Ex_ver3 (Ludwig, 2003).

5.d. Muscovite ^{40}Ar–^{39}Ar dating

^{40}Ar–^{39}Ar measurements were performed at the State Key Laboratory of Lithospheric Evolution, Institute of Geology and Geophysics, Chinese Academy of Sciences (IGGCAS) in Beijing. Details of the method are given by Wang *et al.* (2006*a*, 2007*a*).

Aliquots of mineral separates were wrapped in aluminium foil and stacked in quartz vials along with the neutron flux monitor GA1550 biotite, which has a K–Ar age of 98.5 ± 0.8 Ma (Spell & McDougall, 2003). The samples were irradiated at the H8 position in the 49-2 Reactor at the China Institute of Atomic Energy in Beijing, with a neutron flux of *c.* 6.5×10^{12} n cm^{-2} s^{-1}. Samples were heated stepwise with a double vacuum resistance furnace. Following five additional

https://doi.org/10.1017/S0016756816001096 Published online by Cambridge University Press

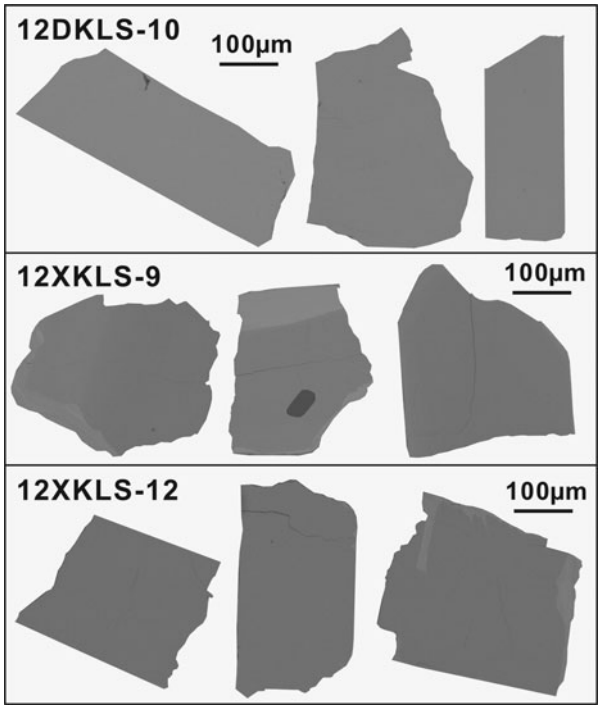

Figure 4. Representative back-scattered electron (BSE) images of columbite-tantalite grains from the Dakalasu (Be-Nb-Ta) and Xiaokalasu (Li-Nb-Ta) pegmatites for *in situ* U–Pb dating.

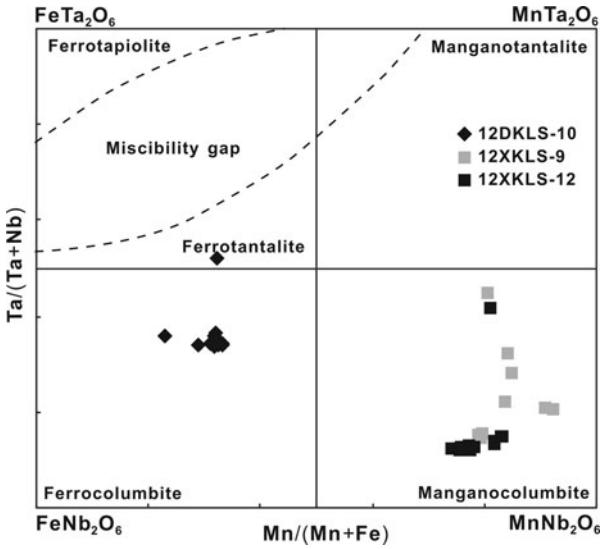

Figure 5. Compositions of columbite-tantalite from the Dakalasu (Be-Nb-Ta) and Xiaokalasu (Li-Nb-Ta) pegmatites.

minutes of released gas purification on Zr–Al getters, the isotopic data were measured using a MM5400 mass spectrometer. After correcting for mass discrimination, system blanks and radiometric interference, ^{40}Ar–^{39}Ar ages were calculated according to $^{40}Ar^{*39}Ar_K$ ratios, and the *J* value was obtained by analyses of the monitors. Plateau ages were determined from three or more contiguous steps comprising >50 % of the ^{39}Ar released, revealing concordant ages at the 95 % confidence level (2σ). The raw data were processed using the ArAr CALC-software of Koppers (2002).

The correction factors of interfering isotopes produced during irradiation were determined by analysis of irradiated pure CaF_2 and K_2SO_4. Mass discrimination was monitored using an on-line air pipette from which multiple measurements were made before and after each incremental-heating experiment. The decay constant used is $\lambda = 5.543 \times 10^{-10}$ a^{-1} (Steiger & Jäger, 1977). All ^{37}Ar abundances were corrected for radiogenic decay (half-life 35.1 days). The uncertainty for each apparent age is given at one standard deviation. The inverse isochrones were calculated from the plateau steps using the York regression algorithm (York, 1969).

6. Results

6.a. Major-element compositions of columbite-tantalite

BSE imaging was used to illustrate chemical heterogeneities for further dating. Representative BSE images of the columbite-tantalite grains from samples 12DKLS-10, 12XKLS-9 and 12XKLS-12 are presented in Figure 4. The columbite-tantalite crystals studied are mainly euhedral and subeuhedral (Fig. 4). Most columbite-tantalite grains from sample 12DKLS-10 are homogeneous, while those from samples 12XKLS-9 and 12XKLS-12 are homogeneous with or without a narrow Ta-rich alteration/growth rim (Fig. 4). The homogeneous targets in the columbite-tantalite grains were primary and selected for U–Pb isotope analyses.

The EMPA results indicate that the columbite-tantalite grains of the Dakalasu (Be-Nb-Ta) pegmatite and the Xiaokalasu (Li-Nb-Ta) pegmatite belong to Fe-columbite and Mn-columbite, respectively (Table 2; Fig. 5). Also, one grain from sample 12DKLS-10 shows a composition of Fe-tantalite (Fig. 5). The Ta/(Nb + Ta) values range from 0.12 to 0.52. The Mn/(Fe + Mn) values are different for the Dakalasu pegmatite (0.23–0.33) and Xiaokalasu pegmatite (0.74–0.92). Compared with the columbite-tantalite grains from the Xiaokalasu pegmatite, those from the Dakalasu pegmatite have higher TiO_2 (2.62–4.41 wt %), WO_3 (2.78–3.61 wt %) and ZrO_2 (0.49–0.88 wt %) concentrations, coupled with lower contents of PbO (≤0.24 wt %). The crystals investigated also contain extremely low amounts of Y_2O_3 (≤0.09 wt %), Sb_2O_3 (≤0.04 wt %) and CaO (≤0.05 wt %).

6.b. LA-ICP-MS columbite-tantalite U–Pb ages

The U–Pb data of columbite-tantalite can be seen in online supplementary Table S1 (available at http://journals.cambridge.org/geo). A total of 14 spot analyses of 12 columbite-tantalite populations from sample 12DKLS-10 were obtained (Fig. 6). The columbite-tantalite grains analysed have extremely high U concentrations (1083–4291 ppm) and variable Th contents (19.24–101.6 ppm) and Th/U ratios (0.018–0.024). The $^{206}Pb/^{238}U$ ratios for these 14 spots

https://doi.org/10.1017/S0016756816001096 Published online by Cambridge University Press

Table 2. The EMPA data averages (wt %) of columbite-tantalite in the Dakalasu (Be-Nb-Ta) and Xiaokalasu (Li-Nb-Ta) pegmatites.

	12DKLS-10 n=12		12XKLS-9 n=13		12XKLS-12 n=14	
	Average	σ	Average	σ	Average	σ
WO_3	3.23	0.26	0.96	0.37	0.87	0.31
Ta_2O_5	38.78	4.07	26.13	9.27	19.33	7.82
Nb_2O_5	36.22	3.60	53.42	8.49	59.20	7.29
TiO_2	3.76	0.54	0.25	0.06	0.46	0.09
ZrO_2	0.71	0.15	0.05	0.03	0.13	0.12
SnO_2	0.30	0.06	0.00	0.01	0.00	0.00
Y_2O_3	0.00	0.01	0.01	0.01	0.01	0.03
Sb_2O_3	0.00	0.01	0.01	0.02	0.01	0.01
FeO	11.81	0.56	3.31	0.92	4.15	0.66
MnO	5.28	0.47	15.34	0.94	15.10	0.63
CaO	0.00	0.00	0.01	0.01	0.01	0.01
PbO	0.09	0.07	0.12	0.06	0.18	0.08
Total	100.18	0.40	99.59	0.96	99.46	0.68
O=6 atoms (apfu)						
W^{6+}	0.052	0.004	0.015	0.007	0.013	0.006
Ta^{5+}	0.659	0.093	0.420	0.178	0.300	0.151
Nb^{5+}	1.157	0.091	1.585	0.190	1.699	0.160
Ti^{4+}	0.176	0.023	0.011	0.003	0.020	0.004
Zr^{4+}	0.022	0.005	0.001	0.001	0.004	0.003
Sn^{4+}	0.008	0.002	0.000	0.000	0.000	0.000
Y^{3+}	0.000	0.000	0.000	0.000	0.000	0.001
Sb^{3+}	0.000	0.000	0.000	0.000	0.000	0.000
Fe^{2+}	0.615	0.027	0.160	0.042	0.194	0.028
Mn^{2+}	0.278	0.025	0.755	0.045	0.717	0.024
Ca^{2+}	0.000	0.000	0.001	0.000	0.001	0.001
Pb^{2+}	0.002	0.001	0.002	0.001	0.003	0.001
Sum B-site	2.072	0.009	2.032	0.006	2.036	0.005
Sum A-site	0.895	0.011	0.918	0.013	0.915	0.013
Mn/(Fe + Mn)	0.31	0.03	0.82	0.05	0.79	0.03
Ta/(Nb + Ta)	0.36	0.05	0.21	0.09	0.15	0.08

yield a weighted mean age of 239.6 ± 3.8 Ma with a MSWD of 2.8 (Fig. 6). A total of 18 analyses of 13 columbite-tantalite grains from sample 12XKLS-9 were obtained (Fig. 6). The U contents are relatively low (307.3–1341 ppm), accompanied with low Th contents (2.79–28.03 ppm) and similar Th/U ratios (0.007–0.022). The 18 spot analyses show a concordia age of 258.1 ± 3.1 Ma with a MSWD of 0.45, and a weighted mean age of 258.4 ± 4.6 Ma with a MSWD of 3.2 (Fig. 6). A total of 18 spots of 14 columbite-tantalite crystals from sample 12XKLS-12 were analysed (Fig. 6). The U, Th contents and Th/U ratios range over 608.4–3270 ppm, 4.71–42.99 ppm and 0.007–0.019, respectively. The 18 spot analyses produce a concordia age of 262.3 ± 2.5 Ma with a MSWD of 0.16, and a weighted mean age of 262.7 ± 3.6 Ma with a MSWD of 2.5 (Fig. 6).

6.c. Zircon characteristics

The zircon populations in samples HST-P, QKE-2-1 and TEL-1 are mainly spongy, euhedral to subhedral grains, with variable sizes (HST-P: 100–161 μm; QKE-2-1: 62–107 μm; TEL-1: 95–207 μm) in CL imaging (Fig. 7). Some zircon grains have oscillatory cores with a black mantle (e.g. grain 15 in sample HST-P) (Fig. 7). Some zircon grains display irregular mantles or heterogeneous rims (e.g. grains 1 and 4 in sample TEL-1) (Fig. 7). These zircon characteristics, especially the spongy and porous parts on CL images, suggest that zircons from the Husite, Qunkuer and Taerlang pegmatites have suffered metamictization or recrystallization, likely due to high U concentrations. This is commonly observed in REL pegmatites (Ding *et al*. 2010; Soman *et al*. 2010).

6.d. LA-ICP-MS zircon U–Pb ages

The analyses of zircon U–Pb dating are shown in online supplementary Table S2 (available at http://journals.cambridge.org/geo). The zircon U–Pb ages are plotted in Figure 8. A total of 18 analyses of 14 zircons from sample HST-P were obtained (Fig. 8). Zircons analysed have variable U concentrations (2743–8408 ppm), Th contents (45.74–2687 ppm) and Th/U ratios (0.014–0.320). The $^{206}Pb/^{238}U$ ratios for these 14 spots yielded a weighted mean age of 198.5 ± 2.5 Ma with a MSWD of 4.3 (Fig. 8). A total of 16 analyses of 16 zircons from sample QKE-2-1 were obtained (Fig. 8). The 16 analyses have variable U concentrations (3548–28581 ppm), Th contents (15.60–248.5 ppm) and Th/U ratios (0.003–0.009). The $^{206}Pb/^{238}U$ ratios for these 16 spots yielded a concordia age of 194.3 ± 1.6 Ma with a MSWD of 2.9, and a weighted mean age of 195.0 ± 2.1 Ma with a MSWD of 2.7 (Fig. 8). A total of 14 analyses of 14

https://doi.org/10.1017/S0016756816001096 Published online by Cambridge University Press

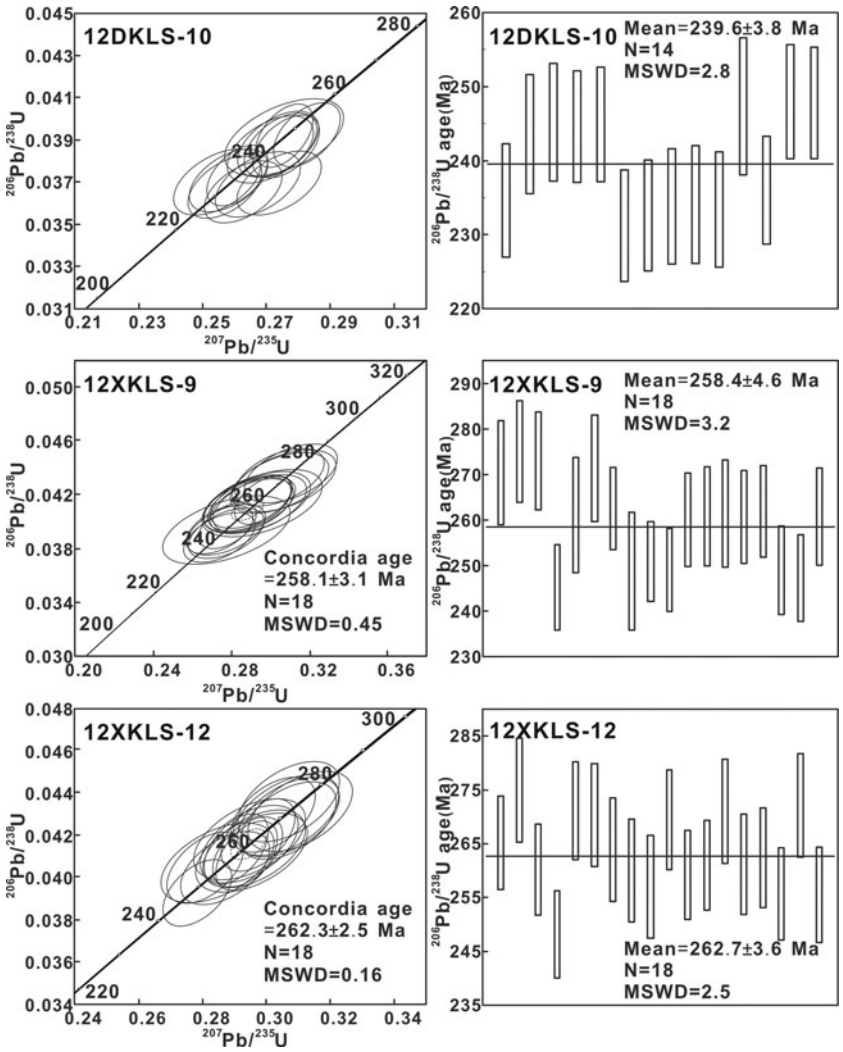

Figure 6. Concordia and weighted mean prism diagrams displaying the LA-ICP-MS U–Pb ages of columbite-tantalite grains from the Dakalasu (Be-Nb-Ta) and Xiaokalasu (Li-Nb-Ta) pegmatites in the Chinese Altai.

zircons from sample TEL-1 were obtained (Fig. 8). Zircons analysed from sample TEL-1 have highly variable U concentrations (3663–20712 ppm), Th contents (28.80–413.7 ppm) and Th/U ratios (0.004–0.068). The $^{206}Pb/^{238}U$ ratios for these 14 points yielded a concordia age of 248.2 ± 2.2 Ma with a MSWD of 7.2 Ma, and a weighted mean age of 247.5 ± 2.6 Ma with a MSWD of 2.6 (Fig. 8).

6.e. Muscovite ^{40}Ar–^{39}Ar ages

^{40}Ar–^{39}Ar dating of muscovite from samples TLT-2, BC-4, KMNG-1, HST-P, QKE-2-1, XKLS-2, WZG-1 and WZG-4 were performed. The muscovite ^{40}Ar–^{39}Ar dating results can be seen in online supplementary Table S3 (available at http://journals.cambridge.org/geo).

The muscovite ^{40}Ar–^{39}Ar dating of sample TLT-2, obtained at temperatures of 800–1300 °C, displays a fairly flat age spectrum with a well-defined plateau, giving a plateau weighted age of 286.4 ± 1.6 Ma (2σ) (MSWD=0.83) and an inverse isochron age of 286.4 ± 2.1 Ma (MSWD=0.94) with over 96.30 % of $^{39}Ar_K$ released (Fig. 9). The ^{40}Ar–^{39}Ar step-heating results (750–1140 °C) of muscovite in sample BC-4 provide a plateau weighted age of 297.0 ± 2.6 Ma (2σ) (MSWD=9.69) and an inverse isochron age of 295.3 ± 2.8 Ma (MSWD=6.78) with 92.23 % of $^{39}Ar_K$ released (Fig. 9). The muscovite ^{40}Ar–^{39}Ar dating of sample KMNG-1 step heated over 700–1230 °C yield a plateau weighted age of 265.2 ± 1.5 Ma (2σ) (MSWD=1.70) and an inverse isochron age of 264.5 ± 1.7 Ma (MSWD=1.26) with 100 % of $^{39}Ar_K$ released (Fig. 9). The muscovite ^{40}Ar–^{39}Ar dating of sample HST-P, obtained at temperatures of 650–1300 °C, shows a fairly flat age spectrum with a well-defined plateau, giving a plateau weighted age of 178.8 ± 1.0 Ma (2σ) (MSWD=1.68) and an inverse isochron age of 178.4 ± 1.4 Ma (MSWD=1.78) with over 100.00 % of $^{39}Ar_K$ released (Fig. 9). The ^{40}Ar–^{39}Ar step-heating results (750–1130 °C) of muscovite in sample QKE-2-1 provide a plateau weighted age of 162.2 ± 0.9 Ma (2σ) (MSWD=0.78) and an inverse isochron age of 162.9 ± 2.5 Ma (MSWD=0.85) with 93.77 % of $^{39}Ar_K$ released (Fig. 9). The muscovite ^{40}Ar–^{39}Ar dating of sample XKLS-2 step

https://doi.org/10.1017/S0016756816001096 Published online by Cambridge University Press

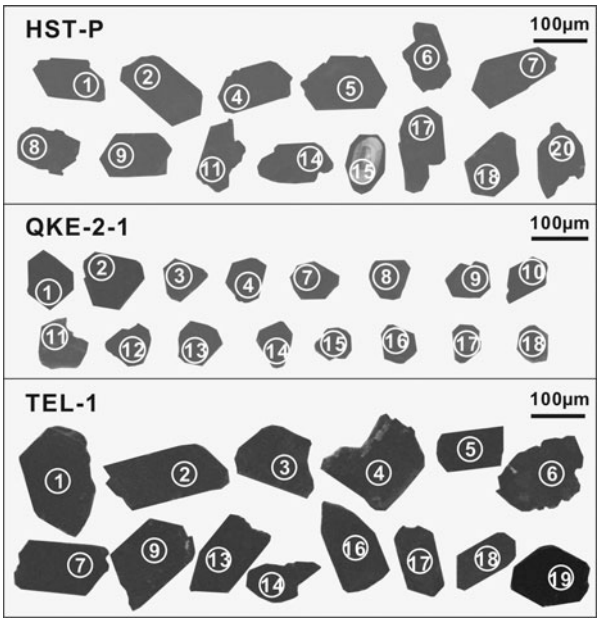

Figure 7. Cathodoluminenscenece (CL) images of dated zircon grains from the Husite (Be), Qunkuer (Be) and Taerlang (barren) pegmatites in the Chinese Altai. Analysed spots are circled and the codes correspond to the results in online supplementary Table S2.

heated over 650–1300 °C gives a plateau weighted age of 237.7 ± 1.3 Ma (2σ) (MSWD=1.45) and an inverse isochron age of 237.6 ± 2.0 Ma (MSWD=1.60) with 100 % of $^{39}Ar_K$ released (Fig. 9). The muscovite ^{40}Ar–^{39}Ar dating of sample TEL-1 step heated over 650–1300 °C produces a plateau weighted age of 231.9 ± 1.2 Ma (2σ) (MSWD=1.11) and an inverse isochron age of 232.0 ± 2.5 Ma (MSWD=1.22) with 82.29 % of $^{39}Ar_K$ released (Fig. 9). The muscovite ^{40}Ar–^{39}Ar dating of sample WZG-4 step heated over 650–1300 °C yields a plateau weighted age of 237.4 ± 1.2 Ma (2σ) (MSWD=0.95) and an inverse isochron age of 237.4 ± 1.4 Ma (MSWD=1.05) with 98.07 % of $^{39}Ar_K$ released (Fig. 9).

The inverse isochron ages of these samples are coincident with corresponding plateau ages (Fig. 9). The analyses forming remarkably flat age plateaus suggest the absence of excess argon or any diffusive argon loss. The ages of 286.4 ± 1.6 Ma, 297.0 ± 2.6 Ma, 265.2 ± 1.5 Ma, 178.8 ± 1.0 Ma, 162.2 ± 0.9 Ma, 237.7 ± 1.3 Ma, 231.9 ± 1.2 Ma and 237.4 ± 1.2 Ma for samples TLT-2, BC-4, KMNG-1, HST-P, QKE-2-1, XKLS-2, TEL-1 and WZG-4 are reliable for the crystallization age of muscovite from the REL pegmatites in the Chinese Altai.

7. Discussion

7.a. Interpretation of columbite-tantalite U–Pb ages

The columbite-tantalite minerals are good targets for U–Pb dating of pegmatites and related mineral deposits (e.g. Romer, Smeds & Černý, 1996; Smith *et al.* 2004; Melcher *et al.* 2008, 2015; Deng *et al.* 2013) because they occur widely in pegmatite dykes (e.g. Černý & Ercit, 1989; Beurlen *et al.* 2008; Linnen, Van Lichtervelde & Černý, 2012; Badanina *et al.* 2015; Melcher *et al.* 2015) and have high U content but low common Pb content (e.g. Romer & Wright, 1992; Romer & Smeds, 1994, 1996, 1997; Romer & Lehmann, 1995). Moreover, the columbite-tantalite minerals are ore minerals in pegmatites which are mineralized by Nb and Ta, and are then considered to be unequivocally bound to the ore-forming system or its remobilization (Romer & Lehmann, 1995). It is advisable to use columbite of textural relation with primary phases in the host pegmatite to obtain an accurate date of the primary columbite generation, because columbite U–Pb age data from primary and secondary columbite differ by 20–30 Ma (Romer & Smeds, 1994; Romer & Lehmann, 1995; Smith *et al.* 2004). In this study, the columbite-tantalite grains are assembled with primary phases and euhedral crystals (Fig. 3). Although some grains are accompanied with weak hydrothermal alteration growths (Fig. 4), the analysed targets are homogeneous parts of the grains. The columbite-tantalite grains are primary and the columbite-tantalite U–Pb dating results that we found are reliable, including a weighted mean age of 239.6 ± 3.8 Ma for the Dakalasu (Be-Nb-Ta) pegmatite and two concordant ages of 258.1 ± 3.1 Ma and 262.3 ± 2.5 Ma for the Xiaokalasu (Li-Nb-Ta) pegmatites. We interpret these ages as the emplacement age and the REL mineralization age of the Dakalasu (Be-Nb-Ta) and Xiaokalasu (Li-Nb-Ta) pegmatites.

The columbite-tantalite U–Pb weighted mean age of 239.6 ± 3.8 Ma is the emplacement age of the Dakalasu (Be-Nb-Ta) pegmatite, since the sample 12DKLS-10 is from wall zone of the pegmatite. Nevertheless, this age does not correspond to the earlier zircon U–Pb age determinations (272.5 ± 1.4 Ma and 270.1 ± 1.7 Ma; Ren *et al.* 2011) and is even later than muscovite ^{40}Ar–^{39}Ar plateau age (248.4 ± 2.1 Ma; Wang *et al.* 2003). Actually, there are many pegmatite dykes located in Dakalasu, some of which are REL mineralized (Zou & Li, 2006). The pegmatite dyke dated in this study and the pegmatites dated previously are possibly distinct dykes, but all in Dakalasu (Fig. 1). On the other hand, the granites which are located around the Dakalasu pegmatites (<10 km) formed in two age ranges of 248 ± 4 Ma (Tong, 2006) and 275–276 Ma (Wang *et al.* 2006*b*; Sun *et al.* 2009*a*) (Fig. 1), indicating that there were at least two magma events. In accordance with these coeval granites, there might be at least two generations of pegmatite formation in the Dakalasu deposit of early Permian and Middle Triassic age.

The samples 12XKLS-9 and 12XKLS-12 come from the intermediate zones of the middle and northern parts of the Xiaokalasu (Li-Nb-Ta) pegmatite (Table 1). The columbite U–Pb concordia ages of 258.1 ± 3.1 Ma (12XKLS-9) and 262.3 ± 2.5 Ma (12XKLS-12) represent Nb-Ta mineralization time

https://doi.org/10.1017/S0016756816001096 Published online by Cambridge University Press

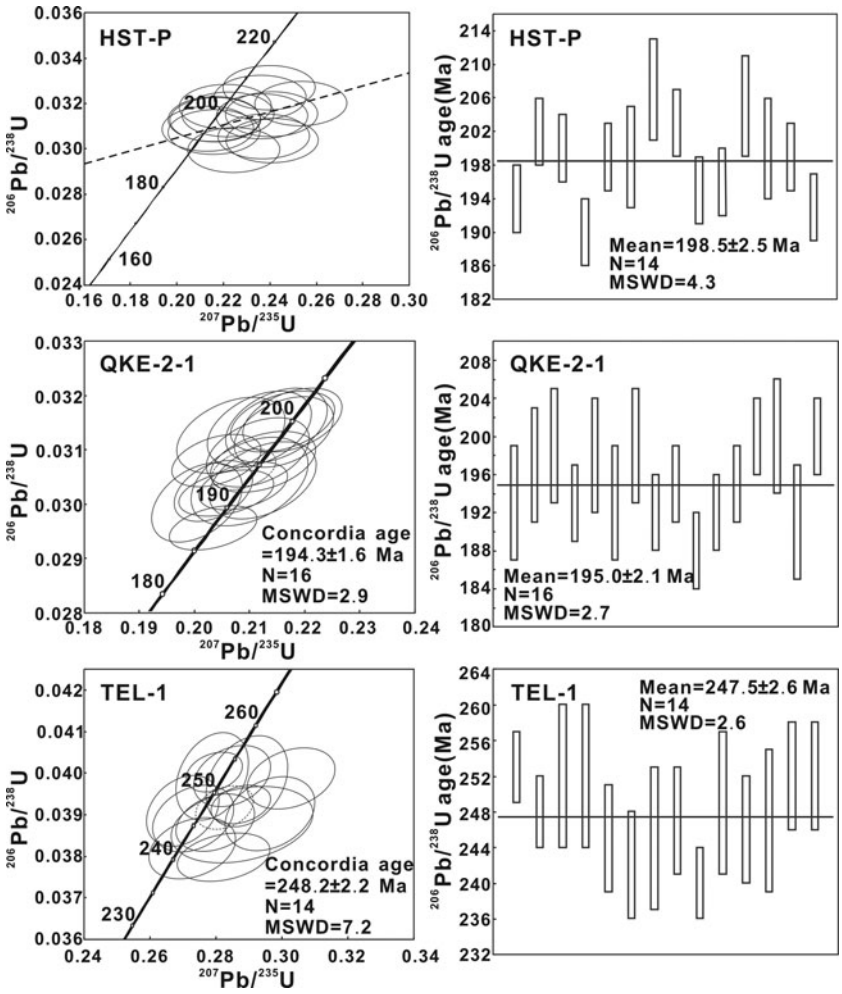

Figure 8. Concordia and weighted mean prism diagrams showing the LA-ICP-MS U-Pb ages of zircon grains from the Husite (Be), Qunkuer (Be) and Taerlang (barren) pegmatites in the Chinese Altai.

which is of middle–late Permian age. The columbite grains in 12XKLS-9 are assembled with fine albites, but those in 12XKLS-12 with coarse albites. These two concordia ages, which are close but different, suggest that the assemblages of fine albites in the intermediate zone are related with replacement and formed later than assemblages of coarse-grained spodumene and albite.

7.b. Interpretation of zircon U–Pb ages

The zircon U–Pb system is commonly used to date the igneous rocks including pegmatite dykes. Although the zircon U–Pb dating of granitic pegmatites has some problems, such as strong metamictization of zircons (Dickin, 1995; Romer Smeds & Černý, 1996), which is possibly caused by extremely high U and Th contents (up to 7.1 wt % U and 2.4 wt % Th; Deng *et al.* 2013) and hydrothermal alteration (Mezger & Krogstad, 1997; Soman *et al.* 2010; Adetunji *et al.* 2016), or containing amounts of inherited zircon (e.g. Marsh *et al.* 2012), the U–Pb zircon geochronometer is one of the most important dating methods for pegmatites (e.g. Wang *et al.* 2007*c*; Liu *et al.* 2010*a*; Lupulscu *et al.* 2011; Ren *et al.* 2011; Deng *et al.* 2013; Zhou *et al.* 2015*a*; Adetunji *et al.* 2016). The zircons analysed here suffered some degree of radiation damage, but they are not inherited (Fig. 7). These zircons were collected from the Be and barren pegmatites which are less fractionated than those of complex REL mineralized (Be-Nb-Ta, Li-Nb-Ta and Li-Be-Nb-Ta-Cs), accordingly accompanied with relatively weak hydrothermal alteration. The zircon U–Pb ages are therefore reliable. They are a weighted mean age of 198.5 ± 2.5 Ma for the Husite (Be) pegmatite and two concordia ages of 194.3 ± 1.6 Ma and 248.2 ± 2.2 Ma for the Qunkuer (Be) pegmatite and Taerlang (barren) pegmatite, respectively. These ages are interpreted as the emplacement ages of pegmatites, since the closure temperature of zircon U–Pb system is close to the temperature of magmatic stage of pegmatites (e.g. Zhu *et al.* 2000). Consequently, the Be pegmatites in the Kelumute–Jideke pegmatite field emplaced during Early Jurassic time, whereas one barren pegmatite in the Xiaokalasu–Qiebielin pegmatite field intruded during Early Triassic time.

7.c. Implications of muscovite ^{40}Ar–^{39}Ar ages

It is commonly believed that a late hydrothermal fluid stage is one of the parts of the formation process of pegmatites (e.g. London, 1986; Lu, Wang & Li, 1997;

https://doi.org/10.1017/S0016756816001096 Published online by Cambridge University Press

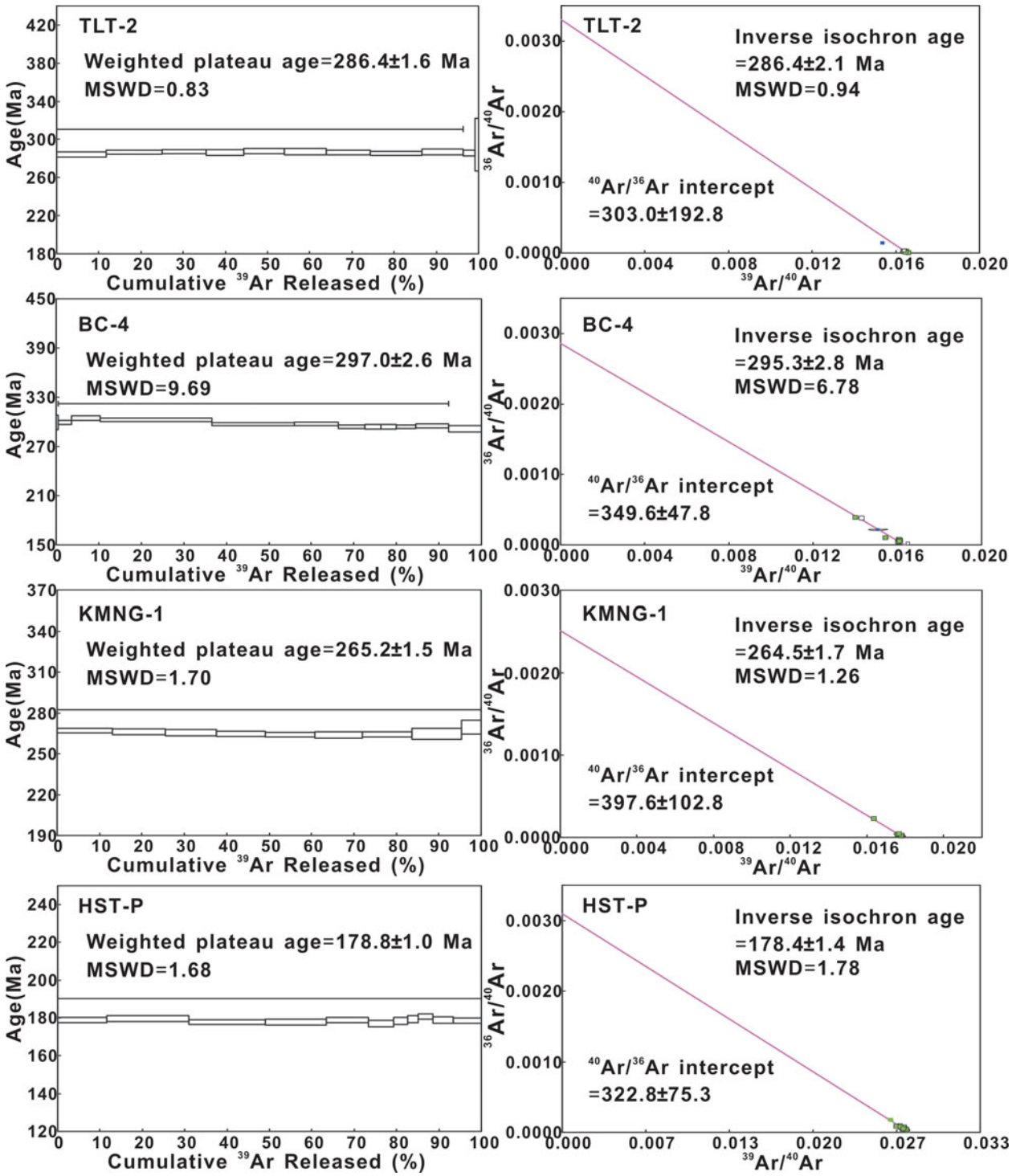

Figure 9. (Colour online) Weighted plateau and inverse isochron ^{40}Ar/^{39}Ar ages of muscovite for the REL pegmatites in the Chinese Altai.

Zou & Li, 2006; Wang *et al*. 2007*b*, 2009*a*; Zhang *et al*. 2008; Zhu *et al*. 2000; Zhou *et al*. 2013, 2015*b*), because pegmatitic magmas are fertile and enriched in H_2O and fluxes (e.g. Jahns & Burnham, 1969; London, 2005, 2009; Simmons & Webber, 2008; London, 2014), leading to increased fluid exsolution during crystallization, fractionation and evolution (e.g. Thomas & Davidson, 2012; Zhang *et al*. 2008; Zhu *et al*. 2000). The closure temperature of Ar–Ar isotope systems of muscovite is low (*c.* 358 °C) (Hames & Bowring, 1994), but close to the temperature of the end stage of pegmatite evolution (*c.* 300–450 °C, e.g. London, 1986; Lu, Wang & Li, 1997). Although muscovite is susceptible to late fluid (Sun & Higgins, 1996), the muscovite ^{40}Ar–^{39}Ar age of pegmatite is closely related to the age of late hydrothermal stage and therefore represents the lower limit of the end of pegmatite formation.

In this study, we found eight muscovite ^{40}Ar–^{39}Ar ages for the typical REL pegmatites in the Chinese

https://doi.org/10.1017/S0016756816001096 Published online by Cambridge University Press

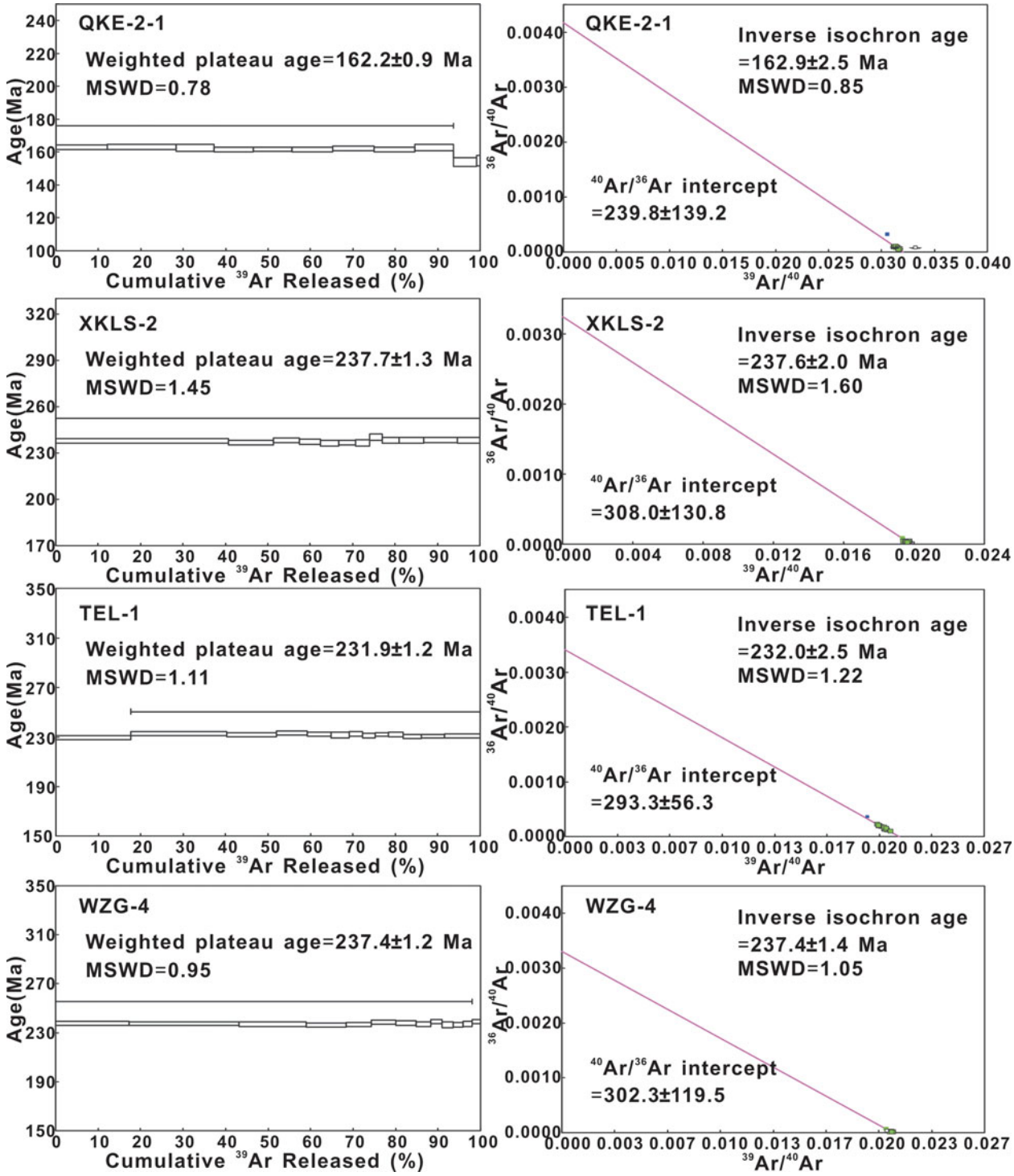

Figure 9. Continued

Altai (Fig. 9). In the Qinghe pegmatite field, the muscovite ^{40}Ar–^{39}Ar plateau ages of the Talate (Li-Be-Nb-Ta), Baicheng (Nb-Ta) and Kangmunagong (barren) pegmatites are 286.4 ± 1.6 Ma, 297.0 ± 2.6 Ma and 265.2 ± 1.5 Ma, respectively, indicating an early–middle Permian REL pegmatite-forming event. In the Kelumute–Jideke pegmatite field, the muscovites from the Husite (Be) and Qunkuer (Be) pegmatites display ^{40}Ar–^{39}Ar plateau ages of 178.8 ± 1.0 Ma and 162.2 ± 0.9 Ma, respectively, suggesting that the end of evolution of these Be pegmatites occurred around Early–Late Jurassic time. The pegmatites in the Xiaokalasu–Qiebielin pegmatite field, including the Xiaokalasu (Li-Nb-Ta), Weizigou (Be) and Taerlang (barren) dykes, have similar muscovite ^{40}Ar–^{39}Ar plateau ages of 237.7 ± 1.3 Ma, 237.4 ± 1.2 Ma and 231.9 ± 1.2 Ma, respectively. The muscovite ^{40}Ar–^{39}Ar plateau ages of the Xiaokalasu (Li-Nb-Ta) in this study are close to that previously reported (233.8 ± 0.4 Ma; Wang *et al*. 2003). The formation of REL pegmatites in the Xiaokalasu–Qiebielin pegmatite field ended around Middle–Late Triassic time.

https://doi.org/10.1017/S0016756816001096 Published online by Cambridge University Press

Table 3. Geochronological results of the REL pegmatites in the Chinese Altai.

Pegmatite field (no.)	Pegmatite deposit	Mineralization type	Age (Ma)	Dating method	Reference
Qiongkuer–Abagong (IV)					
Jiamanhaba (9)	Jiamanhaba	Be	237.5 ± 2.6	I-1	Ren *et al*. 2011
	Jiamanhaba	Be	269.4 ± 1.6	I-1	Ren *et al*. 2011
Hailiutan–Yeliuman (8)	Yeliuman	Be	263.8 ± 1.6	I-1	Ren *et al*. 2011
Xiaokalasu–Qiebielin (7)	Akebasitawu	Be	249.7 ± 0.7	I-1	Ren *et al*. 2011
	Qiebielin	Be	240.5 ± 1.4	I-1	Ren *et al*. 2011
	Xiaokalasu	Li-Nb-Ta	233.8 ± 0.4	V	Wang, Chen & Xu, 2003
	Xiaokalasu	Li-Nb-Ta	258.1∼262.3	II-2	this study
			237.7 ± 1.3	V	this study
	Weizigou	Be	237.4 ± 1.2	V	this study
	Taerlang	Barren	248.2 ± 2.2	I-2	this study
			231.9 ± 1.2	V	this study
Dakalasu–Kekexier (6)	Dakalasu	Be-Nb-Ta	248.4 ± 2.1	V	Wang, Chen & Xu, 2003
	Dakalasu	Be-Nb-Ta	272.5 ± 1.4	I-1	Ren *et al*. 2011
	Dakalasu	Be-Nb-Ta	270.1 ± 1.7	I-1	Ren *et al*. 2011
	Dakalasu	Be-Nb-Ta	239.6 ± 3.8	II-1	this study
Kalaeerqisi (5)	Hulugong	Be-Nb-Ta	246.8 ± 1.2	I-1	Ren *et al*. 2011
Central Altaishan (III)					
Kelumute–Jideke (4)	Azubai	Be-gem	154.1 ± 0.1	V	Wang *et al*. 2000
	Husite	Be-Nb-Ta	244.3 ± 1.1	I-1	Ren *et al*. 2011
	Husite	Be	198.5 ± 2.5	I-1	this study
			178.8 ± 1.0	V	this study
	Qunkuer	Be-Nb-Ta-Cs	199.1 ± 1.0	I-1	Ren *et al*. 2011
	Qunkuer	Li-Be-Nb-Ta-Cs	212.2 ± 1.7	I-1	Ren *et al*. 2011
	Qunkuer	Be-Nb-Ta	206.8 ± 1.6	I-1	Ren *et al*. 2011
	Qunkuer	Be	194.3 ± 1.6	I-2	this study
			162.2 ± 0.9	V	this study
	Kelumute	Li-Be-Nb-Ta	202.9 ± 0.8	I-1	Ren *et al*. 2011
	Kelumute No. 112	Li-Be-Nb-Ta	188.3 ± 1.7	I-1	Lv *et al*. 2012
Keketuohai (2)	Asikaerte	Be	218.2 ± 3.9	I-1	Wang *et al*. 2015
			218.6 ± 1.3	IV	Wang *et al*. 2015
	Keketuohai	Li-Be-Nb-Ta	212.7 ± 2.5	I-1	Ren *et al*. 2011
	Keketuohai	Li-Be-Nb-Ta	190.6 ± 1.2	I-1	Ren *et al*. 2011
	Keketuohai	Li-Be-Nb-Ta	180.7 ± 0.5	I-1	Ren *et al*. 2011
	Keketuohai	West dyke-Be	213 ± 2	I-1	Wang *et al*. 2007*c*
	Koktokay No. 3	Li-Be-Nb-Ta-Rb-Cs-Hf	194.8 ± 2.3	I-1	Wang *et al*. 2007*c*;Zhou *et al*. 2015*a*
			177.9–182.1	V	Chen *et al*. 2000;Zhou *et al*. 2015*a*
			196.4 ± 1.5	III	Zou *et al*. 1986
Qiongkuer–Abagong (IV)					
Qinghe (1)	Bulukete	Be	275.5 ± 4.2	I-1	Ren *et al*. 2011
	Talate	Li-Be-Nb-Ta	286.4 ± 1.6	V	this study
	Baicheng	Nb-Ta	297.0 ± 2.6	V	this study
	Kangmunagong	Barren	265.2 ± 1.5	V	this study

Note: I-1, zircon U–Pb weighted mean ages; I-2, zircon U–Pb concordia ages; II-1, columbite-tantalite weighted mean ages; II-2, columbite-tantalite concordia ages; III, uranmicrolite U–Pb weighted mean ages; IV, molybdenite Re-Os isochron ages; V, muscovite ^{40}Ar–^{39}Ar plateau ages.

7.d. REL pegmatite formation times and their tectonic implications

The previous geochronological studies and the ages in this research of the REL pegmatites (33 pegmatite dykes) in the Chinese Altai are summarized in Table 3. The formation of the REL pegmatites in the Chinese Altai generally continued over early Permian – Late Jurassic time, and is mainly concentrated in strata of early Permian, Middle Triassic and Early Jurassic age (Table 3; Fig. 10). Differently from the muscovite pegmatites which formed in an orogenic setting (e.g. Wang *et al*. 2004), the REL pegmatites in the Chinese Altai mainly formed in a post-orogenic and anorogenic setting.

On the basis of dating for pegmatites mineralized by muscovite, muscovite-REL and REL in the Chinese Altai, it is believed that the more evolved the pegmatites are, the later they formed (Wang *et al*. 2004). However, the pegmatites of various REL mineralization types (e.g. Be, Be-Nb-Ta, Li-Nb-Ta, Li-Be-Nb-Ta-Cs), accompanied with different degrees of fractionation, do not show a unified evolution trend from simple Be type to complex Li-Be-Nb-Ta-Cs type (highly fractionated and evolved) (Fig. 11). The simple Be pegmatites formed during Permian–Jurassic time with a wide age range, and the complex Li-Be-Nb-Ta-Cs pegmatites formed during both Permian and Jurassic time (Table 3; Fig. 11). Regarding the Chinese Altai, the relationship between REL types

https://doi.org/10.1017/S0016756816001096 Published online by Cambridge University Press

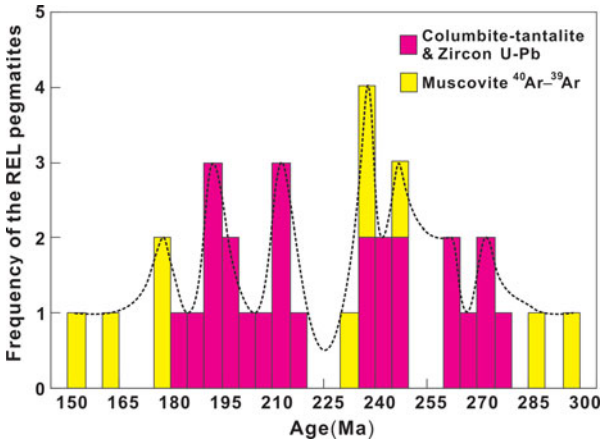

Figure 10. (Colour online) Formation times of the REL pegmatites in the Chinese Altai, shown on the basis of both zircon and columbite-tantalite U–Pb and muscovite ^{40}Ar/^{39}Ar dating results. Only one U–Pb age or one U–Pb age accompanied with a muscovite ^{40}Ar/^{39}Ar age are chosen to represent the formation time for a single REL pegmatite dyke. Age data from Chen *et al*. (2000), Wang *et al*. (2003, 2007), Ren *et al*. (2011), Lv *et al*. (2012), Wang *et al*. (2015), Zhou *et al*. (2015*a*) and this study.

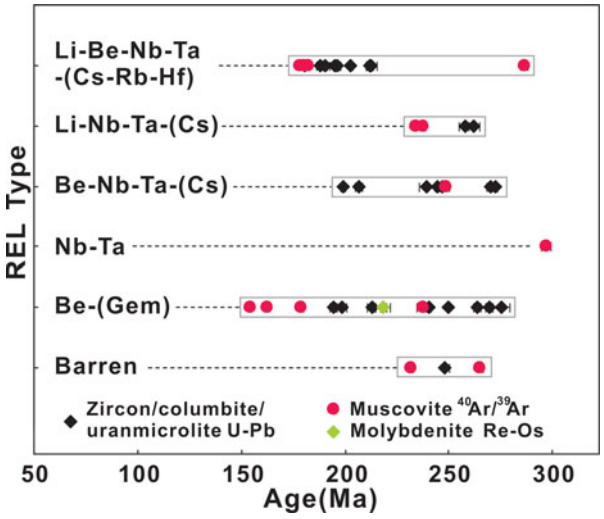

Figure 11. (Colour online) Geochronological data for the REL pegmatites v. REL mineralization types in the Chinese Altai. Data sources: Zou *et al*. (1986), Chen *et al*. (2000), Wang *et al*. (2003, 2007, 2015), Ren *et al*. (2011), Lv *et al*. (2012), Wang *et al*. (2015), Zhou *et al*. (2015*a*) and this study.

(evolution degree) and formation times complicates interpretation.

Actually, the REL pegmatites in the same and adjacent pegmatite fields commonly have similar formation ages in the Chinese Altai (Table 3; Figs 1, 12) and the REL pegmatites are coeval to or formed a little later with granites nearby (Figs 1, 12). In the Central Altaishan terrane, the Koktokay No. 3 pegmatite (Li-Be-Nb-Ta-Rb-Cs-Hf) and the Asikaerte pegmatite (Be) are adjacent to and genetically related to the Aral granite (Zhu, Zeng & Gu, 2006; Cao *et al*. 2013; Liu *et al*. 2014) and the Asikaerte granite (Zou & Li, 2006; Wang *et al*. 2015), respectively, due to similar formation times, evolved compositions and a common source. In the Qiongkuer–Abagong terrane, the Shaerbulake granite (275 ± 2 Ma; Sun *et al*. 2009*a*) and the Dahalasu granite (248 ± 4 Ma; Tong, 2006) are near the Dakalasu pegmatites and coeval to the Be-Nb-Ta pegmatite (270–272 Ma; Ren *et al*. 2011) and Be pegmatite (239.6 ± 3.8 Ma), respectively (Fig. 1). The Mayin'ebo granite (283 ± 4 Ma; Zhou *et al*. 2007) is spatially and temporally close to the Talate (Li-Be-Nb-Ta-Cs) and Baicheng (Nb-Ta) pegmatites (286–297 Ma) (Fig. 1). The formation of REL pegmatites is in correlation with the coeval and nearby granites. The REL pegmatites, which are considered as products of granitic magmatism (e.g. Romer & Lehmann, 1995; Wang *et al*. 2004; Hulsbosch *et al*. 2014), and their coeval and adjacent granites might be products of a common granitic magma activity.

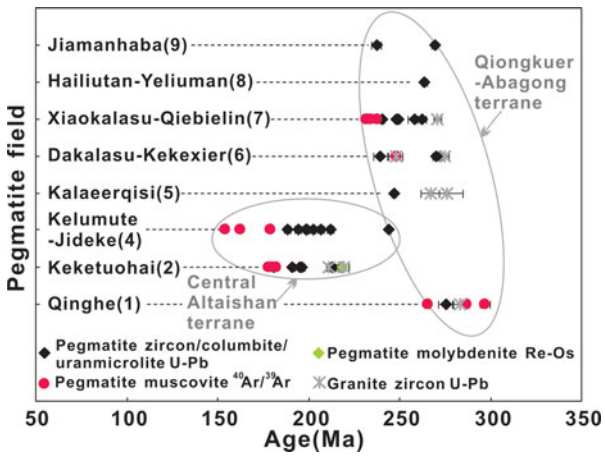

Figure 12. (Colour online) Geochronological data for the REL pegmatites v. pegmatite fields in the Chinese Altai. Data sources: Zou *et al*. (1986), Chen *et al*. (2000), Wang *et al*. (2000, 2003, 2006*b*, 2007, 2015); Tong (2006), Tong *et al*. (2006*a*, *b*), Zhou *et al*. (2007, 2015*a*), Sun *et al*. (2009*a*) , Ren *et al*. (2011), Lv *et al*. (2012), Liu *et al*. (2014) and this study.

The formation of the REL pegmatites and these granites in the Chinese Altai are indicative of the frequent and strong magmatic activities in the post-orogenic and anorogenic setting. It has been determined that the REL pegmatites from Qiongkuer–Abagong terrane (of early Permian – Middle Triassic age) mostly formed earlier than those from Central Altaishan terrane (of Middle Triassic – Jurassic age), and the REL pegmatites in the SE part of Qiongkuer–Abagong terrane (of early–middle Permian age) have older formation ages than others in Qiongkuer–Abagong terrane (middle Permian – Middle Triassic) (Figs 1, 12). The granites that are almost temporally identical to the pegmatites also display a similar formation sequence spatially (Figs 1, 12). Consequently, coupled with the coeval granites, the REL-pegmatite-forming events reflect that the magma activity start from the SE (of early–middle Permian age), then to the NW (of middle Permian – Middle Triassic age), and finally to the central part (of Middle Triassic – Jurassic age) of the Chinese Altai in the post-orogenic and anorogenic setting (Fig. 13).

https://doi.org/10.1017/S0016756816001096 Published online by Cambridge University Press

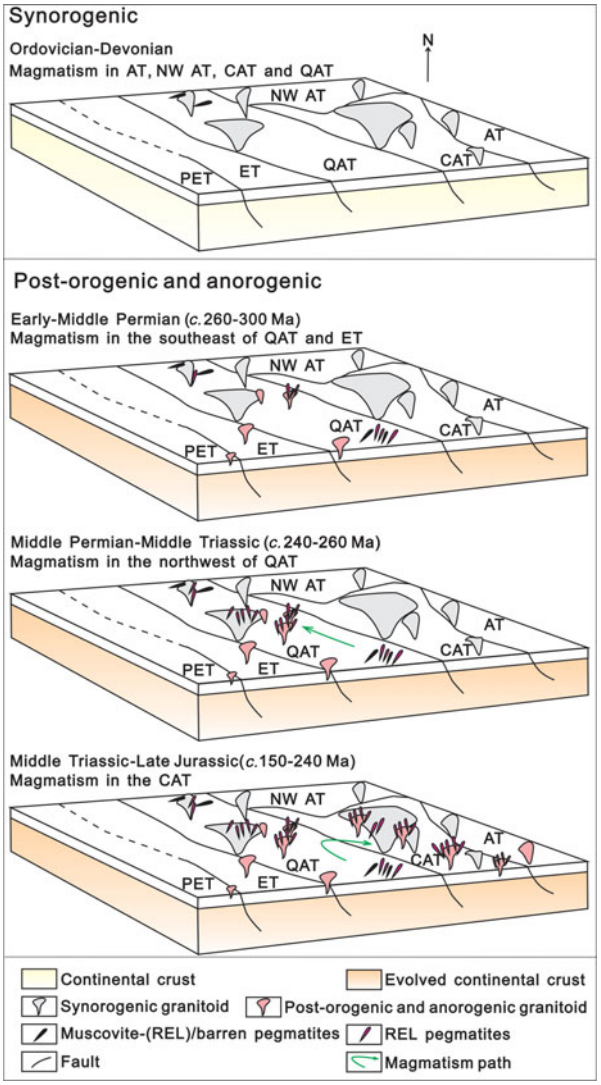

Figure 13. (Colour online) Tectonic implications of geochronological work for the pegmatites in the Chinese Altai. The spatial and temporal distribution of pegmatites and granites reveals the magmatism path of the Chinese Altai during synorogenic and post-orogenic setting. AT – Altaishan terrane; NW AT – NW Altaishan terrane; CAT – Central Altaishan terrane; QAT – Qiongkuer–Abagong terrane; ET – Erqis terrane; PET – Perkin–Ertai terrane.

8. Conclusions

We analysed nine REL pegmatite dykes in the Chinese Altai using LA-ICP-MS columbite-tantalite and zircon U–Pb dating and muscovite ^{40}Ar–^{39}Ar dating methods. (1) The Talate (Li-Be-Nb-Ta), Baicheng (Nb-Ta) and Kangmunagong (barren) pegmatites formed during early–middle Permian time, with muscovite ^{40}Ar–^{39}Ar plateau ages of 286.4 ± 1.6 Ma, 297.0 ± 2.6 Ma and 265.2 ± 1.5 Ma. (2) The Xiaokalasu (Li-Nb-Ta) pegmatite was mineralized by Nb-Ta during late Permian time on the basis of columbite U–Pb concordia ages of 258.1 ± 3.1 Ma and 262.3 ± 2.5 Ma. The Taerlang (barren) pegmatite emplaced during Early Triassic time with a zircon U–Pb concordia age of 248.2 ± 2.2 Ma. The formation of these two pegmatite dykes and the Weizigou (Be) pegmatite ended no later than Middle Triassic time, as shown by muscovite ^{40}Ar–^{39}Ar plateau ages of 237.7 ± 1.3 Ma, 231.9 ± 1.2 Ma and 237.4 ± 1.2 Ma. (3) The Dakalasu (Be-Nb-Ta) pegmatite formed during Middle Triassic time with a zircon weighted mean ^{206}Pb/^{238}U age of 239.6 ± 3.8 Ma, indicating that there are at least two pegmatite-forming events of early Permian and Middle Triassic age. (4) The Husite (Be) and Qunkuer (Be) pegmatites emplaced during Early Jurassic time with a zircon weighted mean ^{206}Pb/^{238}U age of 198.5 ± 2.5 Ma and a concordia age of 194.3 ± 1.6 Ma. The formation ended no later than the Middle Jurassic Period based on muscovite ^{40}Ar–^{39}Ar plateau ages of 178.8 ± 1.0 Ma and 162.2 ± 0.9 Ma.

These new dating results, combined with previously published data, indicate that the formation times of the REL pegmatite in the Chinese Altai span the early Permain – Late Jurassic periods. The REL pegmatites correlated with the coeval and adjacent granites. The REL pegmatites and these granites reflect that magmatic activity continue in the post-orogenic and anorogenic setting, and start from the SE (early–middle Permian), then to the NW (middle Permian – Middle Triassic), and finally to the central part (Middle Triassic – Jurassic) of the Chinese Altai.

Acknowledgements. The work was financially supported by key projects in the National Science and Technology Pillar Program (grant number 2011BAB06B03) and Geology Survey second-level program of China Geological Survey (grant number 121201011000150003). The authors are grateful to Professors Yueheng Yang and Fei Wang for their help with the LA-ICP-MS zircon U–Pb dating and muscovite Ar–Ar dating, respectively. We thank Dr Xudong Che for providing a columbite-tantalite standard (Coltan 139) and valuable suggestions that improved the quality of this manuscript. We also thank Zhenglin Guo, Maode Shen and Xuji Guo for their help with fieldwork.

Supplementary material

To view supplementary material for this article, please visit https://doi.org/10.1017/S0016756816001096.

References

Adetunji, A., Olarewaju, V. O., Ocan, O. O., Ganev, V. Y. & Macheva, L. 2016. Geochemistry and U-Pb zircon geochronology of the pegmatites in Ede area, southwestern Nigeria: a newly discovered oldest Pan African rock in southwestern Nigeria. *Journal of African Earth Sciences* **115**, 177–90.

Armstrong, J. T. 1989. *CITZAF: Combined ZAF and Phirho(Z) Electron Beam Correction Programs*. Pasadena, California: California Institute of Technology.

Badanina, E. V., Sitnikova, M. A., Gordienko, V. V., Melcher, F., Gäbler, H.-E., Lodziak, J. & Syritso, L. F. 2015. Mineral chemistry of columbite-tantalite from spodumene pegmatite of Kolmozero, Kola Peninsula (Russia). *Ore Geology Reviews* **64**, 720–35.

Beurlen, H., Da Silva, M., Thomas, R., Soares, D. & Olivier, P. 2008. Nb-Ta-(Ti-Sn) oxide mineral

chemistry as tracer of rare-element granitic pegmatite fractionation in the Borborema Province, Northeastern Brazil. *Mineralium Deposita* **43**(2), 207–28.

Cai, K. D., Sun, M., Yuan, C., Long, X. P. & Xiao, W. J. 2011*a*. Geological framework and Paleozoic tectonic history of the Chinese Altai, NW China: a review. *Russian Geology and Geophysics* **52**, 1619–33.

Cai, K. D., Sun, M., Yuan, C., Zhao, G. C., Xiao, W. J., Long, X. P. & Wu, F. Y. 2011*b*. Prolonged magmatism, juvenile nature and tectonic evolution of the Chinese Altai, NW China: evidence from zircon U-Pb and Hf isotopic study of Paleozoic granitoids. *Journal of Asian Earth Sciences* **42**, 949–68.

Cao, M. J., Zhou, Q. F., Qin, K. Z., Tang, D. M. & Evans, N. J. 2013. The tetrad effect and geochemistry of apatite from the Altay Koktokay No. 3 pegmatite, Xinjiang, China: implications for pegmatite petrogenesis. *Mineralogy and Petrology* **107**(6), 985–1005.

Černý, P. & Ercit, T. S. 1989. Mineralogy of niobium and tantalum: crystal chemical relationships, paragenetic aspects and their economic implications. In *Lanthanides, Tantalum and Niobium* (eds P. Möller, F. Černý & F. Saupé), pp. 27–79. Berlin: Springer.

Chai, F. M., Dong, L. H., Yang, F. Q., Liu, F., Geng, X. X. & Huang, C. K. 2010. Age, geochemistry and petrogenesis of Tiemierte granites in the Kelang basin at the southern margin of Altay, Xinjiang. *Acta Petrologica Sinica* **26**(2), 377–86 (in Chinese with English abstract).

Che, X. D., Wu, F. Y., Wang, R. C., Gerdes, A., Ji, W. Q., Zhao, Z. H., Yang, J. H. & Zhu, Z. Y. 2015*a*. In situ U-Pb isotopic dating of columbite-tantalite by LA-ICP-MS. *Ore Geology Reviews* **65**, 979–89.

Che, X. D., Wu, F. Y., Wang, R. C., Gerdes, A., Ji, W. Q., Zhao, Z. H., Yang, J. H. & Zhu, Z. Y. 2015*b*. Corrigendum to "In situ U-Pb isotopic dating of columbite-tantalite by LA-ICP-MS". *Ore Geology Reviews* **67**, 400.

Chen, B. & Jahn, B. M. 2002. Geochemical and isotopic studies of the sedimentary and granitic rocks of the Altai orogen of northwest China and their tectonic implications. *Geological Magazine* **139**(1), 1–13.

Chen, F. W., Li, H. Q., Wang, D. H., Cai, H. & Chen, W. 2000. New chronological evidence for Yanshanian diagenetic mineralization in China's Altay orogenic belt. *Chinese Science Bulletin* **45**, 108–14.

Deng, X. D., Li, J. W., Zhao, X. F., Hu, Z. C., Hu, H., Selby, D. & Souza, Z. S. D. 2013. U-Pb isotope and trace element analysis of columbite-(Mn) and zircon by laser ablation ICP-MS: implications for geochronology of pegmatite and associated ore deposits. *Chemical Geology* **344**, 1–11.

Dickin, A. P. 1995. *Radiogenic Isotope Geology*. Cambridge London: University Press, pp. 101–35.

Ding, H. H., Hu, H. H., Zhang, A. C., Ni, P. & Xu, S. J. 2010. Study on metamict zircon from the Koktokay No. 3 granitic pegmatite vein. *Acta Mineralogica Sinica* **32**(2), 160–7.

Gäbler, H.-E., Melcher, F., Graupner, T., Bahr, A., Sitnikova, M. A., Henjes-Kunst, F., Oberthür, T., Brätz, H. & Gerdes, A. 2011. Speeding up the analytical workflow for coltan Fingerprinting fingerprinting by an integrated mineral liberation analysis/LA-ICP-MS approach. *Geostandards and Geoanalytical Research* **35**, 431–48.

Hames, W. E. & Bowring, S. A. 1994. An empirical evaluation of the argon diffusion geometry in muscovite. *Earth and Planetary Science Letters* **124**(1—4), 161–9.

He, G. Q., Han, B. F., Yue, X. J. & Wang, J. H. 1990. *Tectonic Division and Crustal Evolution of the Altai Orogenic Belt in China*. Beijing: Geological House, pp. 9–20 (in Chinese with English abstract). Geoscience of Xinjiang, no. 2.

He, G. Q., Li, M. S., Liu, D. Q. & Zhou, N. H. 1994. *Palaeozoic Crustal Evolution and Mineralization in Xinjiang of China*. Urumqi: Xinjiang People's Publishing House, 437 pp.

Hu, Z. C., Gao, S., Liu, Y. S., Hu, S. H., Chen, H. H. & Huan, H. L. 2008. Signal enhancement in laser ablation ICP-MS by addition of nitrogen in the central channel gas. *Journal of Analytical Atomic Spectrometry* **23**, 1093–101.

Hulsbosch, N., Hertogen, J., Dewaele, S., André, L. & Muchez, P. 2014. Alkali metal and rare earth element evolution of rock-forming minerals from the Gatumba area pegmatites (Rwanda): Quantitative assessment of crystal-melt fractionation in the regional zonation of pegmatite groups. *Geochimica et Cosmochimica Acta* **132**, 349–74.

Jahn, B. M., Wu, F. Y. & Chen, B. 2000*a*. Granitoids of the Central Asian orogenic belt and continental growth in the Phanerozoic. *Earth & Environmental Science Transactions of the Royal Society of Edinburgh* **91**, 181–93.

Jahn, B. M., Wu, F. Y. & Chen, B. 2000*b*. Massive granitoid generation in Central Asia: Nd isotope evidence and implication for continental growth in the Phanerozoic. *Episodes* **23**, 82–92.

Jahns, R. H. & Burnham, C. W. 1969. Experimental studies of pegmatite genesis: I. A model for the derivation and crystallization of granitic pegmatites. *Economic Geology* **64**, 843–64.

Koppers, A. A. P. 2002. ArArCALC-software for $^{40}Ar/^{39}Ar$ age calculations. *Computers & Geosciecnces* **28**, 605–19.

Li, H. J., He, G. Q., Wu, T. R. & Wu, B. 2010. Discovery of the Early Paleozoic post-collisional granite in Altay, China and its geological significance. *Acta Petrologican Sinica* **26**(8), 2445–51 (in Chinese with English abstract).

Li, J. Y., Xiao, W. J., Sun, G. H. & Gao, L. M. 2003. Neoproterozoic-Paleozoic tectonostratigraphy, magmatic activities and tectonic evolution of eastern Xinjiang, NW China. In *Tectonic Evolution and Metallogeny of the Chinese Altay and Tianshan* (eds J. W. Mao, R. J. Goldfarb, R. Seltmann, D. H. Wang, W. J. Xiao & C. Hart), pp. 31–74. London: IAGOD Guidebook Series, CERXCAM/NHM, 10.

Li, T. D. & Poliyangsiji, B. H. 2001. Tectonics and crustal evolution of Altai in China and Kazakhstan. *Xinjiang Geology* **19**, 27–32 (in Chinese).

Linnen, R. L., Van Lichtervelde, M. & Černý, P. 2012. Granitic pegmatites: granitic pegmatites as sources of strategic metals. *Elements* **8**, 275–80.

Liu, F., Yang, F. Q., Mao, J. W., Chai, F. M. & Geng, X. X. 2009. Study on chronology and geochemistry for Abagong granite in Altay orogen. *Acta Petrologica Sinica* **25**(6), 1416–25 (in Chinese with English abstract).

Liu, F., Zhang, Z. X., Li, Q., Zhang, C. & Li, C. 2014. New precise timing constraint for the Keketuohai No. 3 pegmatite in Xinjiang, China and identification of its parental pluton. *Ore Geology Reviews* **56**, 209–19.

Liu, F. L., Robinson, P. T., Gerdes, A., Xue, H. M., Liu, P. H. & Liou, J. G. 2010*a*. Zircon U-Pb ages, REE concentrations and Hf isotope compositions of granitic

leucosome and pegmatite from the north Sulu UHP terrane in China: Constraints on the timing and nature of partial melting. *Lithos* **117**, 247–68.

Liu, G. R., Dong, L. H., Gao, F. P., Chen, J. X., Zhao, H., Wang, D. S., Song, Z. Y., He, L. X. & Qin, J. H. 2010*b*. LA-ICP-MS U-Pb zircon dating and geochemistry of the Devonian granites from the Middle Kelan river valley of Altay in Xinjiang. *Acta Geoscientican Sinica* **31**(4), 519–31 (in Chinese with English abstract).

Liu, W. 1990. Petrogenetic epochs and peculiarities of genetic types of granitoids in the Altai Mts., Xinjiang Uygur Autonomous Region, China. *Geotectonica et Metallogenia* **14**, 43–56 (in Chinese).

Liu, W. 1993. *Whole Rock Isochron Ages of Plutons, Crustal Movements and Evolution of Tectonic Setting in the Altai Mts, Xinjiang Uygur Autonomous Region*. Beijing: Geological House, pp. 35–50 (in Chinese with English abstract). Geoscience of Xinjiang, no. 4.

Liu, W., Liu, C. & Masuda, A. 1997. Complex trace-element effects of mixing-fractional crystallization composite processes: applications to the Alaer granite pluton, Altay Mountains, Xinjiang, northwestern China. *Geological Review* **135**, 103–24 (in Chinese with English abstract).

Liu, W. Z., Zhang, H., Tang, H. F., Tang, Y. & Lv, Z. H. 2015. Molybdenite Re-Os dating of the Asikaerte Be-Mo deposit in Xinjiang, China and its genetic implications. *Geochimica* **44**(2), 145–54 (in Chinese with English abstract).

Liu, Y. S., Gao, S., Hu, Z. C., Gao, C. G. & Wang, D. B. 2010*c*. Continental and oceanic crust recycling-induced melt–peridotite interactions in the Trans-North China Orogen: U-Pb dating, Hf isotopes and trace elements in zircons of mantle xenoliths. *Journal of Petrology* **51**, 537–71.

Liu, Y. S., Hu, Z. C., Gao, S., Günther, D., Xu, J., Gao, C. G. & Chen, H. H. 2008. In situ analysis of major and trace elements of anhydrous minerals by LA-ICP-MS without applying an internal standard. *Chemical Geology* **257**, 34–43.

London, D. 1986. Magmatic-hydrothermal transition in the Tanco rare-element pegmatite: evidence from fluid inclusions and phase-equilibrium experiments. *American Mineralogist* **71**, 376–95.

London, D. 2005. Granitic pegmatites: an assessment of current concepts and directions for the future. *Lithos* **81**, 281–303.

London, D. 2009. The origin of primary textures in granitic pegmatites. *The Canadian Mineralogist* **47**, 697–724.

London, D. 2014. A petrologic assessment of internal zonation in granitic pegmatites. *Lithos* **184–7**, 74–104.

Lu, H. Z., Wang, Z. G. & Li, Y. S. 1997. Magma-fluid transition and the genesis of pegmatite dike No. 3, Altay, Xinjiang, Northwest China. *Chinese Journal of Geochemistry* **16**(1), 43–52.

Luan, S. W., Mao, Y. Y., Fan, L. M., Wu, X. B. & Lin, J. H. 1995. *Selection and Evaluation Research for Lithium-Beryllium-Niobium Prospecting Targets of Keketuohai-Kelumute Area*. Urumqi: The State 305 Project Office, 342 pp (in Chinese).

Ludwig, K. R. 2003. *User's Manual for Isoplot/Ex, Version 3.0: A Geochronological Toolkit for Microsoft Excel*. Berkeley Geochronology Center, Special Publication no. 4, 70 pp.

Lupulscu, M. V., Chiarenzelli, J. R., Pullen, A. T. & Price, J. D. 2011. Using pegmatite geochronology to constrain temporal events in the Adirondack Mountains. *Geosphere* **7**, 23–39.

Lv, Z. H., Zhang, H., Tang, Y. & Guan, S. J. 2012. Petrogenesis and magmatic-hydrothermal evolution time limitation of Kelumute No. 112 pegmatite in Altay, Northwestern China: evidence from zircon U-Pb and Hf isotopes. *Lithos* **154**, 374–91.

Marsh, J. H., Gerbi, C. C., Culshaw, N. G., Johnson, S. E., Wooden, J. L. & Clark, C. 2012. Using zircon U-Pb ages and trace element chemistry to constrain the timing of metamorphic events, pegmatite dike emplacement, and shearing in the southern Parry Sound domain, Grenville Province, Canada. *Precambrian Research* **192–5**, 142–65.

Mei, H. J., Yang, X. C., Wang, J. D., Yu, X. Y., Liu, T. G. & Bai, Z. H. 1993. Trace element geochemistry of late Paleozoic volcanic rocks on the southern side of the Irtysh River and the evolutionary history of tectonic setting. In *Progress of Solid Earth Sciences in Northern Xinjiang, China* (ed. G. Z. Tu), pp. 199–216. Beijing: Science Press (in Chinese).

Melcher, F., Graupner, T., Gäbler, H.-E., Sitnikova, M., Henjes-Kunst, F., Oberthür, T., Gerdes, A. & Dewaele, S. 2015. Tantalum-(niobium-tin) mineralisation in African pegmatites and rare-metal granites: constraints from Nb-Ta oxide mineralogy, geochemistry and U-Pb geochronology. *Ore Geology Reviews* **64**, 667–719.

Melcher, F., Sitnikova, M. A., Graupner, T., Martin, N., Oberthür, T., Henjes-Kunst, F., Gäbler, E., Gerdes, A., Brätz, H., Davis, D. W. & Dewaele, S. 2008. Fingerprinting of conflicet minerals: columbite-tantalite ("coltan") ores. *SGA News* **23**, 1–14.

Mezger, K. & Krogstad, E. J. 1997. Interpretation of discordant U-Pb zircon ages: an evaluation. *Journal of Metamorphic Geology* **15**, 126–40.

Qin, K. Z. 2000. Metallogeneses in relation to Central-Asia style orogeny of Northern Xinjiang. Post-Doctoral Research Report, Institute of Geology and Geophysics, Chinese Academy of Sciences, 195 pp (in Chinese with English abstract).

Qin, K. Z., Xiao, W. J., Zhang, L. C., Xu, X. W., Hao, J., Sun, S., Li, J. L. & Tosdal, R. M. 2005. Eight stages of major ore deposits in northern Xinjiang, NW China: clues and constraints on the tectonic evolution and continental growth of Central Asia. In *Mineral Deposit Research: Meeting the Global Challenge* (eds J. W. Mao & F. P. Bierlein), pp. 1327–30. Proceedings of the Eighth Biennial SGA Meeting Beijing, China, 18–21 August 2005, Springer.

Qu, G. S. & Zhang, J. J. 1991. *Irtys Structural Zone*. Beijing: Geological House, pp. 115–31 (in Chinese with English abstract). Geoscience of Xinjiang, no. 3.

Ren, B. Q., Zhang, H., Tang, Y. & Lv, Z. H. 2011. LA-ICP-MS U-Pb zircon geochronology of the Altai pegmatites and its geological significance. *Acta Mineralogica Sinica* **31**(3), 587–96 (in Chinese with English abstract).

Romer, R. L. & Lehmann, B. 1995. U-Pb columbite age of Neoproterozoic Ta-Nb mineralization in Burundi. *Economic Geology* **90**, 2303–9.

Romer, R. L. & Smeds, S. A. 1994. Implications of U-Pb ages of columbite-tantalites from granitic pegmatites for the Palaeoproterozoic accretion of 1.90-1.85 Ga magmatic arcs to the Baltic Shield. *Precambrian Research* **67**, 141–58.

Romer, R. L. & Smeds, S. A. 1996. U-Pb columbite ages of pegmatites from Sveconorwegian terranes in southwestern Sweden. *Precambrian Research* **76**, 15–30.

Romer, R. L. & Smeds, S. A. 1997. U-Pb columbite chronology of post-kinematic Palaeoproterozoic pegmatites in Sweden. *Precambrian Research* **82**, 85–99.

Romer, R. L., Smeds, S. A. & Černý, P. 1996. Crystal-chemical and genetic controls of U-Pb systematics of columbite-tantalite. *Mineralogy and Petrology* **57**, 243–60.

Romer, R. L. & Wright, J. E. 1992. U-Pb dating of columbites: A geochronologic tool to datemagmatism and ore deposits. *Geochimica et Cosmochimica Acta* **56**, 2137–42.

Sengör, A. M. C., Natalín, B. A. & Burtman, V. S. 1993. Evolution of the Altaid tentonic collage and Paleozoic crustal growth in Eurasia. *Nature* **364**, 299–307.

Shen, X. M., Zhang, H. X., Wang, Q., Wyman, D. A. & Yang, Y. H. 2011. Late Devonian-Early Permian A-type granites in the southern Altay Range, Northwest China: petrogenesis and implications for tectonic setting of "A2-type" granites. *Journal of Asian Earth Sciences* **42**(5), 986–1007.

Simmons, W. B. & Webber, K. L. 2008. Pegmaite genesis: state of the art. *European Journal of Mineralogy* **20**, 421–38.

Smith, S. R., Foster, G. L., Romer, R. L., Tindle, A. G., Kelley, S. P., Noble, S. R., Horstood, M. & Breaks, F. W. 2004. U-Pb columbite-tantalite chronology of rare-element pegmatites using TIMS and laser ablation-multi collector-ICP-MS. *Contributions to Mineralogy and Petrology* **147**, 549–64.

Soman, A., Geisler, T., Tomaschek, F., Grange, M. & Berndt, J. 2010. Alteration of crystaline zircon solid solutions: a case study on zircon from an alkaline pegmatite from Zomba-Malosa, Malawi. *Contributions to Mineralogy and Petrology* **160**(6), 909–30.

Spell, T. L. & McDougall, I. 2003. Characterization and calibration of $^{40}Ar/^{39}Ar$ dating standards. *Chemical Geology* **198**, 189–211.

Steiger, R. H. & Jäger, E. 1977. Subcommission on geochronology: convention on the use of decay constants in geo and cosmochronology. *Earth and Planetary Science Letters* **36**, 359–62.

Sun, G. H., Li, J. Y., Yang, T. N., Li, Y. P., Zhu, Z. X. & Yang, Z. Q. 2009*a*. Zircon SHRIMIP U-Pb dating of two linear granite plutons in southern Altay Mountains and its tectonic implications. *Geology in China* **36**(5), 976–87 (in Chinese with English abstract).

Sun, M., Long, X. P., Cai, K. D., Jiang, Y. D., Wong, P. W., Yuan, C., Zhao, G. C., Xiao, W. J. & Wu, F. Y. 2009*b*. Early Paleozoic ridge subduction in the Chinese Altai: insight from the abrupt change in zircon Hf isotopic compositions. *Science in China Series D: Earth Sciences* **39**, 1–14.

Sun, M., Yuan, C., Xiao, W. J., Long, X. P., Xiao, X., Zhao, G. C., Lin, S. H., Wu, F. Y. & Kröner, A. 2008. Zircon U-Pb and Hf isotopic study of gneissic rocks from the Chinese Altai: progressive accretionary history in the early to middle Paleozoic. *Chemical Geology* **247**, 352–83.

Sun, S. S. & Higgins, N. C. 1996. Neodymium and strontium isotope study of the Blue Tier batholith, NE Tasmania, and its bearing on the origin of tin-bearing alkali feldspar granites. *Ore Geology Reviews* **10**, 339–65.

Thomas, R. & Davidson, P. 2012. Water in granite and pegmatite-forming melts. *Ore Geology Reviews* **46**, 32–46.

Tong, Y. 2006. Geochronology, Origin of the Late Paleozoic granitoids from the Altai Orogen in China and their geological significance. PhD thesis, Chinese Academy of Geological Sciences, Beijing. Published thesis (in Chinese with English abstract).

Tong, Y., Wang, T., Hong, D. W. & Dai, Y. J. 2006*a*. TIMS U-Pb zircon ages of Fuyun post-orogenic linear granite plutons on the southern margin of Altay orogenic belt and their implications. *Acta Petrologica et Mineralogica* **29**(6), 619–41 (in Chinese with English abstract).

Tong, Y., Wang, T., Hong, D. W., Dai, Y. J., Han, B. F. & Liu, X. M. 2007. Ages and origin of the early Devonian granites from the north part of Chinese Altai Mountains and its tectonic implications. *Acta Petrologica Sinica* **23**(8), 1933–44 (in Chinese with English abstract).

Tong, Y., Wang, T., Kovach, V. P., Hong, D. W. & Han, B. F. 2006*b*. Age and origin of Takeshiken postorogenic alkali-rich intrusive rocks in southern Altai, near the Mongolian border in China and its implicaitons for continental growth. *Acta Petrologica et Mineralogica* **22**(5), 1267–78 (in Chinese with English abstract).

Wang, C. L., Qin, K. Z., Tang, D. M., Zhou, Q. F., Shen, M. D., Guo, Z. L. & Guo, X. J. 2015. Geochronology and Hf isotope of zircon for the Arskartor Be-Nb-Mo deposit in Altay and its geological implications. *Acta Petrologica Sinica* **31**(8), 2337–52 (in Chinese with English abstract).

Wang, D. H., Chen, Y. C., Li, H. Y., Xu, Z. G. & Li, T. D. 1998. Mantle degassing of the Altai orogenic belt: insight from helium isotope study. *Chinese Science Bulletin* **43**(23), 2541–4 (in Chinese).

Wang, D. H., Chen, Y. C. & Xu, Z. G. 2001. Chronological study of Caledonian metamorphic pegmatite muscovite deposits in the Altay Mountains, northwestern China, and its significance. *Acta Geological Sinica* **75**(3), 419–25 (in Chinese with English abstract).

Wang, D. H., Chen, Y. C. & Xu, Z. G. 2003. $^{40}Ar/^{39}Ar$ isotope dating on muscovite from Indosinian rare metal deposits in Central Altay, Northwestern China. *Bulletin of Mineralogy, Petrology and Geochemistry* **22**(1), 14–7 (in Chinese with English abstract).

Wang, D. H., Chen, Y. C., Zou, T. R., Xu, Z. G., Li, H. Q., Chen, W., Chen, F. W. & Tian, F. 2000. $^{40}Ar/^{39}Ar$ dating for the Azubai rare metal-gem deposit in Altay, Xinjiang: New evidence for Yanshanian mineralization of rare metals. *Geological Review* **46**(3), 307–11 (in Chinese with English abstract).

Wang, D. H., Zou, T. R., Xu, Z. G., Yu, J. J. & Fu, X. F. 2004. Advance in the study of using pegmatite deposits as the tracer of orogenic process. *Advances in Earth Science* **19**(3), 614–20 (in Chinese with English abstract).

Wang, F., Lu, X. X., Lo, C. H., Wu, F. Y., He, H. Y., Yang, L. K. & Zhu, R. X. 2007*a*. Post-collisional, potassic monzonite-minette complex (Shahewan) in the Qinling Mountains (central China): $^{40}Ar/^{39}Ar$ thermochronology, petrogenesis, and implications for the dynamic setting of the Qinling orogen. *Journal of Asian Earth Sciences* **31**(2), 153–66.

Wang, F., Zhou, X. H., Zhang, L. C., Ying, J. F., Zhang, Y. T., Wu, F. Y. & Zhu, R. X. 2006*a*. Late Mesozoic volcanism in the Great Xin'an Range (NE China): timing and implications for the dynamic setting of NE Asia. *Earth and Planetary Science Letters* **251**, 179–98.

Wang, R. C., Che, X. D., Zhang, W. L., Zhang, A. C. & Zhang, H. 2009*a*. Geochemical evolution and late re-equilibration of Na-Cs-rich beryl from the Koktokay #3 pegmatite (Altai, NW China). *European Journal of Mineralogy* **21**, 795–809.

Wang, R. C., Hu, H., Zhang, A. C., Fontan, F., Parseval, P. D. & Jiang, S. Y. 2007*b*. Cs-dominant polylithionite in the Koktokay #3 pegmatite, Altai, NW China: in situ

micro-characterization and implication for the storage of radioactive cesium. *Contributions to Mineralogy and Petrology* **153**, 355–67.

Wang, T., Hond, D. W., Jahn, B. M., Tong, Y., Wang, Y. B., Han, B. F. & Wang, X. X. 2006*b*. Timing, petrogenesis and setting of Paleozoic syn-orogenic intrusions from the Altai Mountains, NW China: Implications for tectonic evolution of an accretionary orogen. *Journal of Geology* **114**, 735–51.

Wang, T., Hong, D. W., Tong, Y., Han, B. F. & Shi, Y. R. 2005. Zircon U-Pb SHRIMP age and origin of post-orogenic Lamazhao granitic pluton from Altai orogen: its implications for vertical continental growth. *Acta Petrologica Sinica* **21**(3), 640–50 (in Chinese with English abstract).

Wang, T., Jahn, B. M., Kovach, V. P., Tong, Y., Hong, D. W. & Han, B. F. 2009*b*. Nd-Sr isotopic mapping of the Chinese Altai and implications for continental growth in the Central Asian Orogenic Belt. *Lithos* **110**, 359–72.

Wang, T., Tong, Y., Jahn, B. M., Zou, T. R., Wang, Y. B., Hong, D. W. & Han, B. F. 2007*c*. SHRIMP U-Pb Zircon geochronology of the Altai No. 3 Pegmatite, NW China, and its implications for the origin and tectonic setting of the pegmatite. *Ore Geology Reviews* **32**, 325–36.

Wang, T., Tong, Y., Li, S., Zhang, J. J., Shi, X. J., Li, J. Y., Han, B. F. & Hong, D. W. 2010. Spatial and temporal variations of granitoids in the Altay orogen and their implications for tectonic setting and crustal growth: perspectives from Chinese Altay. *Acta Petrologica et Mineralogica*, **29**(6), 595–618 (in Chinese with English abstract).

Wang, X. J., Zou, T. R., Xu, J. G., Yu, X. Y. & Qiu, Y. Z. 1981. *Study of Pegmatite Minerals of the Altai Region*. Beijing: Science Press, 140 pp (in Chinese).

Wiedenbeck, M., Alle, P., Corfu, F., Griffin, W., Meier, M., Oberli, F., Quadt, A. V., Roddick, J. & Spiegel, W. 1995. Three natural zircon standards for U-Th-Pb, Lu-Hf, trace element and REE analyses. *Geostandards Newsletter* **19**, 1–23.

Windley, B. F., Alexeiev, D., Xiao, W. J., Kröner, A. & Badarch, G. 2007. Tectonic models for accretion of the Central Asian Orogenic Belt. *Journal of the Geological Society* **164**, 31–47.

Windley, B. F., Kröner, A., Guo, J., Qu, G., Li, Y. & Zhang, C. 2002. Neoproterozoic to Paleozoic geology of the Altai orogen, NW China: new zircon age data and tectonic evolution. *Journal of Geology* **110**, 719–37.

Xiao, W. J., Windley, B. F., Badarch, G., Sun, S., Li, J. L., Qin, K. Z. & Wang, Z. 2004. Palaeozoic accretionary and convergent tectonics of the southern Altaids: implications for the growth of central Asia. *Journal of the Geological Society, London* **161**, 339–42.

Xiao, W. J., Windley, B. F., Yuan, C., Sun, M., Han, C. M., Lin, S. F., Chen, H. L., Yan, Q. R., Liu, D. Y., Qin, K. Z., Li, J. L. & Sun, S. 2009. Paleozoic multiple subduction-accretion processes of the southern Altaids. *American Journal of Science* **309**, 221–70.

Xiao, X. C., Tang, Y. Q., Feng, Y., Zhu, B., Li, J. & Zhou, M. 1992. Tectonics in northern Xinjiang and its neighbouring areas. Beijing: Geological Publishing, 171 pp (in Chinese with English abstract).

Xie, L. W., Zhang, Y. B., Zhang, H. H., Sun, J. F. & Wu, F. Y. 2008. In situ simultaneous determination of trace elements, U-Pb and Lu-Hf isotopes in zircon and baddeleyite. *Chinese Science Bulletin* **53**, 1565–73.

York, D. 1969. Least squares fitting of a straight line with correlated errors. *Earth and Planetary Science Letters* **5**, 320–4.

Yuan, C., Sun, M., Long, X. P., Xia, X. P., Xiao, W. J., Li, X. H., Lin, S. F. & Cai, K. D. 2007*a*. Constraining the deposition time and tectonic background of the Habahe Group of the Altai. *Acta Petrologica Sinica* **23**(7), 1635–44 (in Chinese with English abstract).

Yuan, C., Sun, M., Xiao, W. J., Li, X. H., Chen, H. L., Lin, S. F., Xia, X. P. & Long, X. P. 2007*b*. Accretionary orogenesis of the Chinese Altai: insights from Palaeozoic granitoids. *Chemical Geology* **242**, 22–39.

Zhang, A. C., Wang, R. C., Jiang, S. Y., Hu, H. & Zhang, H. 2008. Chemical and textural features of tourmaline from the spodumene-subtype Koktokay No. 3 pegmatite, Altai, northwestern China: a record of magmatic to hydrothermal evolution. *The Canadian Mineralogist* **46**, 41–58.

Zhang, X. B., Sui, J. X., Li, Z. C., Liu, W., Yang, X. Y., Liu, S. S. & Huang, H. Y. 1996. *Evolution of the Erqis Structural Belt and Mineralization*. Beijing: Science Press, 205 pp (in Chinese).

Zhao, Z. H., Wang, Z. G., Zou, T. R. & Masuda, A. 1993. The REE, isotopic composition of O, Pb, Sr and Nd and petrogenesis of granitoids in the Altai region. In *Progress of Solid-Earth Sciences in Northern Xinjiang, China* (ed. G. Z. Tu), pp. 239–66. Beijing: Science Press (in Chinese with English abstract).

Zhou, G., Zhang, Z. C., Luo, S. B., He, B, Wang, X., Yin, L. J., Zhao, H., Li, A. H. & He, Y. K. 2007. Confirmation of high-temperature strongly peraluminous Mayin'ebo granites in the south margin of Altay, Xinjiang: age, geochemistry and tectonic implications. *Acta Petrologica Sinica* **23**(8), 1909–20 (in Chinese with English abstract).

Zhou, Q. F., Qin, K. Z., Tang, D. M., Ding, J. G. & Guo, Z. L. 2013. Mineralogy and significance of micas and feldspars from the Koktokay No. 3 pegmatitic rare-element deposit, Altai. *Acta Petrologica Sinica* **29**(9), 3004–22 (in Chinese with English abstract).

Zhou, Q. F., Qin, K. Z., Tang, D. M., Tian, Y., Cao, M. J. & Wang, C. L. 2015*a*. Formation age and evolution time span of the Koktokay No. 3 pegmatite, Altai, NW China: evidence from U-Pb zircon and $^{40}Ar/^{39}Ar$ muscovite ages. *Resource Geology* **65**(3), 210–31.

Zhou, Q. F., Qin, K. Z., Tang, D. M., Wang, C. L., Tian, Y. & Sakyi, P. A. 2015*b*. Mineralogy of the Koktokay No. 3 pegmatite, Altai, NW China: implications for evolution and melt-fluid processes of rare-metal pegmatites. *European Journal of Mineralogy* **27**, 433–57.

Zhu, J. C., Wu, C. N., Liu, C. S., Li, F. C., Huang, X. L. & Zhou, D. S. 2000. Magmatic-hydrothermal evolution and genesis of Koktokay No. 3 rare metal pegmatite dyke, Altai, China. *Geological Journal of China Universities* **6**(1), 40–52 (in Chinese with English abstract).

Zhu, Y. F., Zeng, Y. S. & Gu, L. B. 2006. Geochemistry of the rare metal-bearing pegmatite No. 3 vein and related granites in the Keketuohai region, Altay Mountains, northwest China. *Journal of Asian Earth Sciences* **27**, 61–77.

Zou, T. R., Cao, H. Z. & Wu, B. Q. 1989. Orogenic and anorogenic granitoids of Altay Mountains of Xinjiang and their discrimination criteria. *Acta Geologica Sinica* **2**, 45–64 (in Chinese with English abstract).

Zou, T. R. & Li, Q. C. 2006. *Rare and Rare Earth Metallic Deposits in Xinjiang, China*. Beijing: Geological Publishing House, 284 pp (in Chinese with English abstract).

Zou, T. R., Zhang, X. C., Jia, F. Y., Wang, R. C., Cao, H. Z. & Wu, B. Q. 1986. The origin of No. 3 pegmatite in Altaishan, Xinjiang. *Mineral Deposits* **5**(4), 34–48 (in Chinese with English abstract).

https://doi.org/10.1017/S0016756816001096 Published online by Cambridge University Press